Joint Antenna Position and Beamforming Optimization for Movable Antenna-Enabled Secure IRS-ISAC Network

Xiaowen Cao, *Member, IEEE*, Peng Jiang, Guangxu Zhu, *Member, IEEE*, Yejun He, *Senior Member, IEEE*, and Mohsen Guizani, *Fellow, IEEE*

***Abstract*—Integrated sensing and communication (ISAC) can effectively improve the spectrum utilization rate and enhance the system performance. This paper focuses on the secure communication problem in an ISAC system, which consists of a base station (BS), a legitimate user, an eavesdropping target, and an intelligent reflecting surface (IRS). To further investigate the impact of channel reconfigurability on the security performance of the ISAC system, movable antennas (MA) are employed at the BS instead of traditional fixed antennas. We aim to jointly design the communication transmit beamforming at the BS, the sensing covariance matrix, the phase shifts of the IRS, and the positions of the MAs to ensure secure communication for the user equipment (UE), subject to the constraints including the maximum transmit power at the BS, the constant-modulus constraint of the IRS, the minimum spacing requirement between MAs, and the sensing beam gain constraint. To address the non-convex optimization problem, we adopt an alternating optimization algorithm. Specifically, by combining successive convex approximation (SCA) and semidefinite relaxation (SDR) techniques, the problems of designing the transmit beamforming matrix at the BS and the phase shifts of the IRS are transformed into convex optimization problems. Then, a particle swarm optimization (PSO) algorithm is used to optimize the positions of MAs. Simulation results demonstrate the effectiveness of the IRS in improving the system performance and highlight the superiority of MAs in improving security compared to traditional ISAC systems.**

***Index Terms*—Integrated sensing and communication, movable antenna, intelligent reflecting surface, physical layer security, particle swarm optimization.**

Received 20 May 2025; revised 21 August 2025; accepted 9 September 2025. Date of publication 24 September 2025; date of current version 24 December 2025. This work was supported in part by the National Key Research and Development Program of China under Grant 2023YFE0107900, in part by the National Natural Science Foundation of China under Grant 62501407, Grant 62371313, and Grant U2541208, in part by Shenzhen Science and Technology Program under Grant RCBS20231211090520032, in part by Guangdong Young Talent Research Project under Grant 2023TQ07A708, in part by the Guangdong Provincial Key Laboratory of Future Networks of Intelligence under Grant 2022B1212010001, in part by the Shenzhen Key Program of Natural Science Foundation under Grant JCYJ20241202124219023, and in part by the program of Shenzhen Key Laboratory Evaluation under Grant SYSPG 20241211173908022. Recommended for acceptance by Dr. Weijie Yuan. *(Corresponding author: Yejun He.)*

Xiaowen Cao is with the State Key Laboratory of Radio Frequency Heterogeneous Integration, Sino-British Antennas and Propagation Joint Laboratory of MOST, Guangdong Engineering Research Center of Base Station Antennas and Propagation, Shenzhen Key Laboratory of Antennas and Propagation, College of Electronics and Information Engineering, Shenzhen University, Shenzhen 518060, China, and also with the Guangdong Provincial Key Laboratory of Future Networks of Intelligence, The Chinese University of Hong Kong, Shenzhen 518172, China (e-mail: caoxwen@szu.edu.cn).

Peng Jiang and Yejun He are with the State Key Laboratory of Radio Frequency Heterogeneous Integration, Sino-British Antennas and Propagation Joint Laboratory of MOST, Guangdong Engineering Research Center of Base Station Antennas and Propagation, Shenzhen Key Laboratory of Antennas and Propagation, College of Electronics and Information Engineering, Shenzhen University, Shenzhen 518060, China (e-mail: 1044609737@qq.com; heyejun@126.com).

Guangxu Zhu is with the Shenzhen Research Institute of Big Data, Shenzhen 518172, China (e-mail: gxzhu@sribd.cn).

Mohsen Guizani is with the Mohamed Bin Zayed University of Artificial Intelligence, Abu Dhabi 7909, UAE (e-mail: mguizani@ieee.org).

Digital Object Identifier 10.1109/TNSE.2025.3613825

I. Introduction

NEXT-GENERATION wireless networks demand substantially enhanced sensing and communication capabilities to support a plethora of emerging applications [1]. To enhance the high-precision sensing prowess within wireless systems, integrated sensing and communication (ISAC), widely acknowledged as one of the pivotal enabling technologies for sixth-generation (6G) wireless networks, has attracted remarkable attention and spurred extensive researches [2], [3], [4]. A promising emerging research direction in ISAC is edge perception [5], which refers to the integration of ISAC with edge learning [6], [7]. This fusion brings AI-driven sensing and decision-making capabilities closer to end devices, laying the foundation for advanced applications such as smart manufacturing, autonomous vehicles, and intelligent transportation systems. Related work [8], [9], [10] focused on edge computing scenarios and the field of integration of communication and intelligence, committed to improving the efficiency and stability of systems. However, to implement ISAC in practice, it still faces some challenges. First, the physical-layer trade-offs between communication and sensing (such as detection and communication [11] or estimation and communication [12]) are hard to be characterized within a uniform framework, due to the different resource allocation requirements like in spatial degrees of freedom. Then, ISAC systems may inherit vulnerabilities from conventional wireless networks, leading to a degradation in sensing accuracy or misleading perception-driven applications.

In particular, physical layer security (PLS) has gained attraction as a promising approach to safeguard transmissions by leveraging the randomness and spatial diversity inherent in wireless channels [13], [14]. Existing techniques, such as artificial noise injection [15], channel-based secret key generation [16], and cooperative jamming [17] have been widely adopted to

enhance security in wireless networks. Meanwhile, secure beamforming [18] also plays a central role by precisely shaping the transmission pattern to enhance the desired signal quality, thus ensuring confidentiality at the physical layer. However, traditional secure beamforming designs mainly rely on fixed position antennas (FPA), where the positions of the antennas at the transmitter/receiver cannot be changed [19]. This brings a drawback, that is, when the direction of the eavesdropper is close to the azimuth angle at which the legitimate user receives the signal, the channel correlation between the user and the eavesdropping channel will increase significantly [20], making it difficult for the beamforming technology to distinguish between legitimate and illegal users. Therefore, a novel antenna technology called movable antenna (MA) has been proposed in some research. Specifically, MA connected to the radio frequency link through a flexible cable and enabled to move via a mechanical device [21], simultaneously provides additional degrees of freedom.

In ISAC systems, intelligent reflecting surfaces are often considered as key technologies for reconfiguring the propagation links [22]. Through the independent tuning of passive reflecting elements, IRS adjusts incident electromagnetic waves to adapt to the variations in the wireless environment, thereby achieving coverage expansion [23], channel quality improvement [24], and interference mitigation [25]. In situations where the direct line-of-sight (LoS) path between the base station, the user, and the target is obstructed, establishing a virtual LoS link via the IRS can enhance the stability and reliability of a signal transmission. Additionally, through the passive beamforming design of IRS elements, it can further boost the gain for legitimate communication users while decreasing the gain for illegal targets.

IRS-assisted ISAC systems have become a research hotspot in both academia and industry. Leveraging the tunable characteristics of IRS on wireless channels, this technology can effectively enhance the joint communication and sensing performance of ISAC systems: on the one hand, it can expand the applicable scenarios of the system by utilizing the property of diffracting obstacles; on the other hand, it can optimize the system efficiency through dynamic resource scheduling and expand the signal coverage area. However, IRS-assisted ISAC systems still face many challenges, such as high complexity of the channel estimation and complexity of the system-level interference management. It is worth noting that the dynamic regulation capability of IRS on channel characteristics also provides a new technical path for improving the security performance of ISAC systems.

A. Related Work

1) PLS: In research related to PLS, some research attempts are committed to ensuring the security performance of the system by maximizing the secrecy energy efficiency [26], [27]. Specifically, in [26], the secrecy energy efficiency of primary users was guaranteed by jointly designing the artificial noise vector and discrete phase shift of the IRS. Furthermore, the work in [27] considered a visible light communication network and focused on exploring the approach to optimize the performance of secrecy energy efficiency. The authors in [28] discussed ensuring the security of unmanned aerial vehicle (UAV) communication through cooperative jamming and trajectory control, while they further considered a power adaptation scheme in the 3D state and introduced multi-point cooperation [29]. Furthermore, the work in [30] investigated the security transmission problem in UAV-assisted mobile edge computing based on reinforcement learning. Assisted by IRS technology, the work [32] optimized the security performance in a healthcare network with the assistance of the IRS, while authors in [31] used a hybrid deep reinforcement learning method to address the security issues in air-ground communication, improving the communication security performance through multi-UAV cooperation. From the perspective of jamming and beamforming in communication security, robust security of UAV communication is achieved through the design of jamming beamforming in [33], and [34] combined the IRS with non-orthogonal multiple access (NOMA) to achieve secure transmission through adaptive jamming beamforming. The advantages of IRS-UAV for ISAC and related typical technologies are introduced, and different optimization schemes are proposed to address jamming and eavesdropping attacks [35]. Taking into account the imperfect sensing estimation, it could provide a more in-depth research direction for communication security [36].

In some relevant studies on the security performance of ISAC systems, the authors in [37] and [38] considered the scenario where the targets are eavesdroppers and assumed that the non-ideal channel state information can be obtained, which proposed a robust scheme for ISAC systems to improve secure communication and sensing services. The systems studied are mainly in the state where communication and sensing operate independently rather than cooperatively. In the cooperative state, authors in [39] proposed a secure transmission of ISAC systems by optimizing resource allocation design.

2) IRS-Aided ISAC Secure Transmission: Currently, there have been many studies utilizing the IRS to assist in enhancing the security performance of the ISAC system [40], [41], [42], [43], [44], [45], [46], [47], [48], [49], [50]. In specific, the study in [40] proposed a semi-passive IRS-aided ISAC scheme. For both scenarios of point targets and extended targets, it aims to maximize the secrecy rate while minimizing the Cramér-Rao bound (CRB). In the research on the combination of UAVs and the ISAC network, the work in [41] deployed the IRS on UAVs. By leveraging the high-altitude characteristics of UAVs, LoS links were established, thus expanding the coverage area. Moreover, another investigation [42] combined the ISAC base station (BS) with UAVs, enhanced the signal strength through the IRS, and jointly optimized phase shifts of the IRS and the trajectories of the UAVs. In scenarios where the LoS links are obstructed, the authors in [43] utilized the links established by the IRS to realize the virtual LoS link surveillance of illegal targets that are difficult for the BS to detect. Additionally, the research in the non-orthogonal multiple access system [44], through jointly designing the phase shifts of the IRS and artificial jamming, can achieve target detection while ensuring the secure communication of users. In the work [45], the authors studied the IRS-aided ISAC system, taking into account multistatic cooperative sensing. By utilizing the shared azimuth angles, they achieved the localization of the eavesdropping target. Based on the positioning information obtained from the sensing, they optimized the communication transmission beamforming to realize secure communication. The authors in [46] and [47] utilized the simultaneously transmitting and reflecting reconfigurable

TABLE I
COMPARISON OF RELATED WORKS WITH OUR WORK

Reference	IRS	MA	ISAC	Security	Objective Function	Sensing Metric	Communication Metric	Optimization Method
[26]	✓	×	×	✓	Communication metric	–	Secrecy energy efficiency	DRL
[27]	×	×	×	✓	Communication metric	–	Secrecy rate	SCA
[31]	✓	×	×	✓	Communication metric	–	Secrecy rate	DRL
[33]	×	×	×	✓	Communication metric	–	Sum secrecy rate	SCA/SDR
[40]	✓	×	✓	✓	Communication metric	CRB	Secrecy rate	SCA/SDR
[42]	✓	×	✓	✓	Communication metric	Echo SNR	Sum secrecy rate	SCA
[43]	✓	×	✓	✓	Communication metric	Echo SNR	Sum secrecy rate	SCA
[44]	✓	×	✓	✓	Sensing metric	Beam pattern gain	SINR	Penalty-based
[45]	✓	×	✓	✓	Communication metric	Estimated localization	Sum secrecy rate	SCA
[50]	✓	×	✓	✓	Communication metric	Echo SINR	Secrecy rate	DRL
[51]	×	✓	×	✓	Communication metric	–	Beam gain	Closed form
[52]	×	✓	×	✓	Communication metric	–	Secrecy rate	Gradient descent
[53]	×	✓	×	×	Communication metric	–	Sum data rate	SCA
[54]	×	✓	×	×	Communication metric	–	Transmit power	Generalized Benders
[57]	✓	✓	✓	×	Both metrics	–	Sum communication rate	KKT/DCA
[58]	×	✓	✓	×	Sensing metric	CRB	SINR	SCA
[59]	✓	✓	✓	×	Sensing metric	–	SINR	SCA
Proposed	✓	✓	✓	✓	Communication metric	Beam pattern gain	Secrecy rate	SCA/PSO

Note: DGA: Direct gradient descent; KKT: Karush-Kuhn-Tucker.

intelligent surface (STAR) to enhance the security performance of the IRS-ISAC system. The authors in [48] and [49] replace the passive IRS with the active IRS, achieving the phase modulation of the incident signal and simultaneously amplifying the signal. Furthermore, the soft-actor critical algorithm in reinforcement learning was applied to enhance the security of IRS-supported ISAC systems as described in [50].

3) Beamforming and Position Optimization for MA: Current research on MA-assisted communication systems mainly centers on two crucial aspects, i.e., beamforming design [51], [52] and MA position optimization [53], [54]. The seminal work [19] proposed a channel estimation framework for MA systems based on field responses. It also developed a computational method to analyze channel responses under different MA setups within factory environments.

Moreover, recent studies have combined MA with IRS to leverage channel reconfigurability. The work in [55] presented a coordinated MA-IRS system that reduces the user-side signal-to-interference-plus-noise ratio (SINR) by dynamically positioning antennas on IRS surfaces. The authors in [56] explored enhancements for Internet of Things (IoT) networks through joint MA-IRS reconfiguration strategies, which dynamically reshape propagation environments to enhance channel conditions.

Existing studies have systematically explored the spatial advantages of MA in ISAC systems. These investigations demonstrate significant benefits, including enhanced sensing beam gain [57], [58], [59], [60] and optimized communication performance under sensing constraints [61], [62], [63]. Specifically, the work [58] implemented MA configurations at both BS and user terminals, deriving MA position relationships and formulating a constrained CRB minimization problem. Under the constraint of communication SINR, authors in [59] and [60] respectively achieved the maximization of the radar SINR and the maximization of the minimum radar beam gain, through the joint optimization of transmit beamforming and antenna positions. The authors in [61] proposed an effective framework to enhance the communication SINR and the beam pattern gain. The work in [62] achieved a significant improvement in the communication rate and sensing mutual information of ISAC compared to fixed uniform arrays. The bistatic ISAC analysis in [63] decomposed a joint optimization into four coupled subproblems using MA arrays and dual performance metrics. However, in the studies mentioned above, the impact of the channel reconfigurability introduced by MA and IRS on the security performance of ISAC systems has not been thoroughly investigated. The comparison between related work and our work is shown in Table I.

B. Motivation and Contribution

To comprehensively harness the synergistic channel reconfigurability offered by IRS and MA, this paper delves into the realm of secure communication within IRS-enabled ISAC systems with MA. In these systems, the ISAC BS deployed with MA, is tasked with the dual challenge of detecting potential targets that may concurrently function as eavesdroppers and ensuring the uninterrupted communication with legitimate users. Additionally, given that the LoS paths between the BS, the user, and the target are obstructed by physical blockers, the reconstruction of the communication link through the IRS becomes imperative. The contributions of this paper are summarized as follows.

- We aim to jointly optimize the transmit beamforming vector, IRS phase shift configuration, and BS-mounted MA positions, while satisfying the maximum transmit power constraints, IRS unit-modulus phase shift constraints, antenna displacement spatial constraints, and minimum beam pattern gain constraints. The inherent strong coupling among optimization variables induces non-convex interdependencies in the objective function, rendering the joint optimization problem mathematically intractable.
- To tackle the above challenge, we propose an alternating optimization algorithm. The original problem is decoupled into two subproblems, which respectively target the joint

transmit beamforming, IRS phase shift design, and antenna position optimization. Specifically, when the positions of MAs are fixed, the first subproblem is further decomposed into two mutually coupled modules. In the first sub-module, the successive convex approximation (SCA) and semidefinite relaxation (SDR) techniques are utilized to transform the primary problems into tractable convex subproblems. Subsequently, based on the obtained transmit beamforming matrix, SCA and sparse reconstruction conjugate rank (SRCR) techniques are combined to transform the IRS phase shift design problem into a convex problem. Finally, a particle swarm optimization (PSO) based algorithm is used to perform a metaheuristic-driven stochastic search, iteratively optimizing the positions of MAs based on the given beamforming vectors and IRS phase shifts.

- The simulation results demonstrate the effectiveness of the MAs-assisted IRS-ISAC system in enhancing security. Meanwhile, compared with the traditional FPA, it can achieve higher security performance.

C. Organization

The remainder of this paper is structured as follows. Section II details the system model and formulates the associated problems. Subsequently, in Section III, we put forward the proposed algorithm. Moving on to Section VI, simulations are carried out to showcase the performance of the proposed solution. Finally, the conclusion is presented in Section VII.

Notation: The bold-face lower-case and upper-case letters denote the vectors and matrices, respectively. $|a|$ represents the absolute value of a. $\mathrm{diag}\{\boldsymbol{a}\}$ represents a diagonal matrix where the elements of vector $\boldsymbol{a}$ are placed on the main diagonal. $(\cdot)^T$ and $(\cdot)^H$ represent the transpose and hermitian transpose, respectively. $\lfloor\cdot\rfloor$ denotes the floor function. $\mathbb{E}(\cdot)$ denotes the statistical expectation. $\mathcal{CN}(0,\sigma^2)$ represents a complex circularly symmetric Gaussian distribution with a mean of zero and a variance of σ^2. $\mathrm{Tr}(\mathbf{A})$ represents the trace operation of matrix $\mathbf{A}$. $[\cdot]^+=\max\{\cdot,0\}$. $\nabla^H_{\mathbf{W}} f(\mathbf{W},\mathbf{R}_r)$ represents the conjugate transpose of the gradient of the function $f(\cdot)$ with respect to the matrix $\mathbf{W}$.

II. System Model

As shown in Fig. 1, we consider a secure IRS-ISAC system, where the ISAC BS needs to communicate with a user under the assistance of an IRS and sense an environmental target. A BS equipped with a linear MA transmit array of length J, along which the positions of M antennas can be adjusted flexibly. While the BS communicates with the legitimate user called Bob equipped with a single antenna, it needs to sense the target located at the non-line-of-sight (NLoS) link. Assume that the target called Eve also has a single antenna and attempts to intercept Bob's data. Direct links between the BS and the user/target are assumed to be unfavorable due to blockages. As a result, the IRS is responsible for generating strong virtual LoS links to support communication and sensing performance. We further assume that the IRS is a uniform planar array with N reflecting elements. The antenna position vector of the linear MA array in the BS is represented as $\mathbf{t}=\left[t_1,t_2,\ldots,t_M\right]^T\in\mathbb{R}^M$, where t_m denotes the coordinates of the m-th antenna. We define the sets of MAs and IRS as $\mathcal{M}=\{1,\ldots,M\}$ and $\mathcal{N}=\{1,\ldots,N\}$, respectively. To mitigate the mutual coupling between antennas of finite size, a minimum distance $d_{\min}$ is imposed between any two antennas which is given by

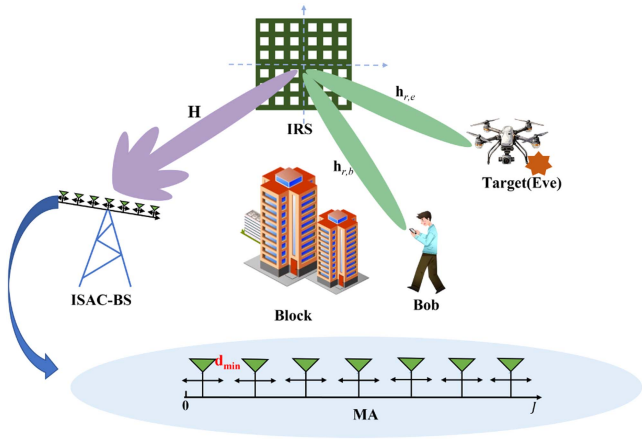

Fig. 1. Illustration of the IRS-ISAC system, where the BS is equipped with MAs.

$$|t_i-t_j|\geq d_{\min},\forall i,j\in\mathcal{M},i\neq j. \tag{1}$$

A. Channel Model

Considering the planar far-field channel model, each transmit/receive path within the same channel shares a common angle of departure, angle of arrival, and path response coefficient, but with distinct signal phases. For simplicity, it is assumed that all channels undergo quasi-static flat-fading and the CSI of all channels involved is perfectly known at both the BS and the IRS. Thus, the channel between the IRS and the BS can be expressed as $\mathbf{H}(\mathbf{t})=\mathbf{G}(\mathbf{t})^H\mathbf{\Lambda}^H\mathbf{F}\in\mathbb{C}^{M\times N}$. The notations mentioned are defined as

- $\mathbf{G}(\mathbf{t})=[\mathbf{G}_1(t_1),\ldots,\mathbf{G}_m(t_m),\ldots,\mathbf{G}_M(t_M)]\in\mathbb{C}^{L\times M}$ is the transmit field response vector (FRV) in the BS, where L denotes the number of channel paths between the BS and the IRS. Each $\mathbf{G}_m\in\mathbb{C}^{L\times 1}$ corresponds to the transmit FRV from the m-th MA and the IRS for $m\in\mathcal{M}$.
- $\mathbf{G}_m(t_m)=[e^{j\frac{2\pi}{\lambda}t_m\cos\theta_{m,1}},\ldots,e^{j\frac{2\pi}{\lambda}t_m\cos\theta_{m,L}}]^H$, where $\theta_{m,l}\in[0,2\pi]$ is the elevation angles of the l-th path for the m-th antennas for $l=1,\ldots,L$, and λ is the wavelength.
- $\mathbf{\Lambda}=\mathrm{diag}\{[\nu_1,\ldots,\nu_L]\}\in\mathbb{C}^{L\times L}$, where ν_l is the complex response of the path l.
- $\mathbf{F}=[\mathbf{f}(\mathbf{r}_1),\ldots,\mathbf{f}(\mathbf{r}_n),\ldots,\mathbf{f}(\mathbf{r}_N)]\in\mathbb{C}^{L\times N}$ is the receive FRV of the IRS, and $\mathbf{r}_n=(x_n,y_n)$ represents the n-th coordinates of the reflection element. $\mathbf{f}(\mathbf{r}_n)=[e^{j\frac{2\pi}{\lambda}\rho_r^1(\mathbf{r}_n)},e^{j\frac{2\pi}{\lambda}\rho_r^2(\mathbf{r}_n)},\ldots,e^{j\frac{2\pi}{\lambda}\rho_r^L(\mathbf{r}_n)}]^T\in\mathbb{C}^{L\times 1}$, where $\rho_r^i(\mathbf{r}_n)=x_n+\sin\theta_i^r\cos\psi_i^r+y_n\cos\theta_i^r$ is the difference in the propagation distance of the signal for the i-th receiving path between the position of the element $\mathbf{r}_n$ and the origin of the IRS. Here, ψ_i^r and θ_i^r are the elevation and azimuth angles of the i-th receiving path at the IRS, respectively.

The channel between the IRS to Bob $\mathbf{h}_{r,b} \in \mathbb{C}^{N\times 1}$ follows the Rician fading, which is given by

$$\mathbf{h}_{r,b} = \sqrt{\iota d_{r,b}^{-2.2}}\left(\sqrt{\frac{\kappa}{\kappa+1}}\mathbf{h}_{r,b}^{\mathrm{LoS}} + \sqrt{\frac{1}{\kappa+1}}\mathbf{h}_{r,b}^{\mathrm{NLoS}}\right), \quad (2)$$

where ι denotes the path loss factor at the reference distance $\iota_0 = 1$ m, $d_{r,b}$ represents the distance between the IRS and Bob, κ stands for the Rician factor, and $\mathbf{h}_{r,b}^{\mathrm{NLoS}} \sim \mathcal{CN}(0, \mathbf{I})$ denotes the NLoS component. Given the azimuth $\theta_{r,b} \in (0, 2\pi]$ and the elevation angle $\zeta_{r,b} \in (-\pi/2, \pi/2]$ from the IRS to the user, in accordance with [64], the LoS component is expressed as $\mathbf{h}_{r,b}^{\mathrm{LoS}}$, and its n-th elements $[\mathbf{h}_{r,b}^{\mathrm{LoS}}]_n$ is given by

$$[\mathbf{h}_{r,b}^{\mathrm{LoS}}]_n = e^{j2\pi d_r\left(\lfloor\frac{n}{N_x}\rfloor\eta_{b,1}+(n-\lfloor\frac{n}{N_x}\rfloor N_x)\eta_{b,2}\right)/\lambda}, \forall n \in \mathcal{N}, \quad (3)$$

where $\eta_{b,1} = \sin(\theta_{r,b})\sin(\zeta_{r,b})$, $\eta_{b,2} = \sin(\theta_{r,b})\cos(\zeta_{r,b})$, N_x denotes the number of IRS elements in each row, and d_r is the space between adjacent reflecting elements.

Assume that the virtual LoS channel created by the IRS is stronger than the NLoS channel. Let $\theta_{r,e}$ and $\zeta_{r,e}$ represent the azimuth angle and departure angle of the target relative to the IRS, respectively. Similarity, the steering vector between the IRS and the target can be expressed as $\boldsymbol{a} \in \mathbb{C}^{N\times 1}$, and its n-th element steering vector $[\boldsymbol{a}]_n$ is given by

$$[\boldsymbol{a}]_n = e^{j2\pi d_r\left(\lfloor\frac{n}{N_x}\rfloor\eta_{e,1}+(n-\lfloor\frac{n}{N_x}\rfloor N_x)\eta_{e,2}\right)/\lambda}, \forall n \in \mathcal{N}, \quad (4)$$

where $\eta_{e,1} = \sin(\theta_{r,e})\sin(\zeta_{r,e})$, $\eta_{e,2} = \sin(\theta_{r,e})\cos(\zeta_{r,e})$. Thus, the channel between the IRS and Eve can be expressed as $\mathbf{h}_{r,e} = \sqrt{\iota d_{r,e}^{-2.2}}\boldsymbol{a}(\theta_{r,e}, \zeta_{r,e}) \in \mathbb{C}^{N\times 1}$, where $d_{r,e}$ represents the distance.

B. Signal Model

Let $s_c \sim \mathcal{CN}(\mathbf{0}, 1)$ represent the communication signal transmitted to Bob, $\mathbf{x}_r \in \mathbb{C}^{M\times 1}$ denote the sensing signal vector, which is generated independently of the communication signals. The covariance matrix of $\mathbf{x}_r$ is

$$\mathbf{R}_r \triangleq \mathbb{E}(\mathbf{x}_r\mathbf{x}_r^H) \succeq 0. \quad (5)$$

The transmit signal of the ISAC BS is represented as

$$\mathbf{x} = \mathbf{w}_c s_c + \mathbf{x}_r, \quad (6)$$

where $\mathbf{w}_c \in \mathbb{C}^{M\times 1}$ denote the beamforming matrices for the communication. The covariance matrix $\mathbf{R}_x$ of the transmitted signal $\mathbf{x}$ can be expressed as

$$\mathbf{R}_x = \mathbb{E}(\mathbf{x}\mathbf{x}^H) = \mathbf{w}_c\mathbf{w}_c^H + \mathbf{R}_r. \quad (7)$$

The beamforming gain defined by $\mathcal{P}(\mathbf{w}_c, \mathbf{R}_r, \boldsymbol{\Phi}, \mathbf{t})$ in the sensing direction $\theta_{r,e}$ is adopted to measure the radar performance and can be expressed as

$$\begin{aligned}\mathcal{P}(\mathbf{w}_c,\mathbf{R}_r,\boldsymbol{\Phi},\mathbf{t}) &= \mathbb{E}\left(\left|\mathbf{h}_{r,e}^H\boldsymbol{\Phi}\mathbf{H}(\mathbf{t})^H\mathbf{x}\right|^2\right)\\ &= \mathbf{h}_{r,e}^H\boldsymbol{\Phi}\mathbf{H}(\mathbf{t})^H(\mathbf{w}_c\mathbf{w}_c^H+\mathbf{R}_r)\mathbf{H}(\mathbf{t})\boldsymbol{\Phi}^H\mathbf{h}_{r,e}, \quad (8)\end{aligned}$$

where $\boldsymbol{\Phi} = \mathrm{diag}(\varphi_1, \ldots, \varphi_n, \ldots, \varphi_N)$ represents the phase shift matrix of the IRS with $\varphi_n = \xi_n e^{j\vartheta_n}$, $\xi_n \in [0, 1]$ represents the amplitude reflection coefficient, and $\vartheta_n \in (0, 2\pi]$ denotes the phase shift of the n-th reflecting element. For simplicity, the amplitude effect of the IRS is ignored, i.e., $\xi_n = 1, \forall n \in \mathcal{N}$ [65].

The received signal at Bob and Eve can be obtained as

$$y_i = \mathbf{h}_i^H\boldsymbol{\Phi}\mathbf{H}(\mathbf{t})^H\mathbf{x} + n_i, i \in \{b, e\}, \quad (9)$$

where n_b and n_e hollow the distribution with $\mathcal{CN}(0, \sigma^2)$ represent the received noise at Bob and Eve, respectively. Let $\mathbf{h}_b(\boldsymbol{\Phi}, \mathbf{t}) = \mathbf{H}(\mathbf{t})\boldsymbol{\Phi}^H\mathbf{h}_{r,b}$ and $\mathbf{h}_e(\boldsymbol{\Phi}, \mathbf{t}) = \mathbf{H}(\mathbf{t})\boldsymbol{\Phi}^H\mathbf{h}_{r,e}$ denote the equivalent channels from the BS to Bob and the BS to Eve, respectively. Then, the achievable data rate $R_b(\mathbf{w}_c, \mathbf{R}_r, \boldsymbol{\Phi}, \mathbf{t})$ for Bob can be expressed as

$$R_b(\mathbf{w}_c,\mathbf{R}_r,\boldsymbol{\Phi},\mathbf{t}) = \log_2\left(1+\frac{\left|\mathbf{h}_b(\boldsymbol{\Phi},\mathbf{t})^H\mathbf{w}_c\right|^2}{\mathbf{h}_b(\boldsymbol{\Phi},\mathbf{t})^H\mathbf{R}_r\mathbf{h}_b(\boldsymbol{\Phi},\mathbf{t})+\sigma^2}\right). \quad (10)$$

Similarly, the eavesdropping data rate $R_e(\mathbf{w}_c, \mathbf{R}_r, \boldsymbol{\Phi}, \mathbf{t})$ for Eve to intercept the information intended for Bob is given by

$$R_e(\mathbf{w}_c,\mathbf{R}_r,\boldsymbol{\Phi},\mathbf{t}) = \log_2\left(1+\frac{\left|\mathbf{h}_e(\boldsymbol{\Phi},\mathbf{t})^H\mathbf{w}_c\right|^2}{\mathbf{h}_e(\boldsymbol{\Phi},\mathbf{t})^H\mathbf{R}_r\mathbf{h}_e(\boldsymbol{\Phi},\mathbf{t})+\sigma^2}\right). \quad (11)$$

Thus, the system's secure rate $R_{sec}(\mathbf{w}_c, \mathbf{R}_r, \boldsymbol{\Phi}, \mathbf{t})$ is formulated as

$$R_{sec}(\mathbf{w}_c,\mathbf{R}_r,\boldsymbol{\Phi},\mathbf{t}) = [R_b(\mathbf{w}_c,\mathbf{R}_r,\boldsymbol{\Phi},\mathbf{t}) - R_e(\mathbf{w}_c,\mathbf{R}_r,\boldsymbol{\Phi},\mathbf{t})]^+ \quad (12)$$

C. Problem Formulation

The objective in this work is to maximize the secure rate by jointly designing the transmit beamforming $\mathbf{w}_c$, the covariance matrix $\mathbf{R}_r$, the phase shift matrix $\boldsymbol{\Phi}$, and the MA's position $\mathbf{t}$.

$$\begin{aligned}(\mathrm{P1}): \max_{\mathbf{w}_c,\mathbf{R}_r,\boldsymbol{\Phi},\mathbf{t}} \; & R_{sec}(\mathbf{w}_c, \mathbf{R}_r, \boldsymbol{\Phi}, \mathbf{t})\\ \text{s.t.} \quad & \mathcal{P}(\mathbf{w}_c, \mathbf{R}_r, \boldsymbol{\Phi}, \mathbf{t}) \geq \varepsilon, && (13a)\\ & \|\mathbf{w}_c\|^2 + \mathrm{Tr}(\mathbf{R}_r) \leq P_{\max}, && (13b)\\ & \mathbf{R}_r \succeq \mathbf{0}, && (13c)\\ & \boldsymbol{\Phi} = \mathrm{diag}(e^{j\vartheta_1}, \ldots, e^{j\vartheta_N}), && (13d)\\ & |t_i - t_j| \geq d_{\min}, \forall i, j \in \mathcal{M}, i \neq j, && (13e)\\ & t_m \in [0, J], \forall m \in \mathcal{M}. && (13f)\end{aligned}$$

The radar beamforming gain is specified in the constraint (13a), where ε represents the minimum required radar beamforming. Constraint (13b) denotes the transmission power budget at the BS, with $P_{\max}$ representing the maximum transmission power. Additionally, constraint (13d) addresses the phase shift constraints of the IRS, while constraints (13e) and (13f) represent the MA position constraints. It is observed that the problem (P1) is highly non-convex due to the non-convex objective functions and constraints among coupling variables.

III. Problem Optimization

In this part, we divide the original problem into two subproblems. Specifically, under any given antenna position, we optimize $\mathbf{w}_c, \mathbf{R}_r, \boldsymbol{\Phi}$, by leveraging the SDR and SCA techniques. Then, with the obtained $\mathbf{w}_c, \mathbf{R}_r, \boldsymbol{\Phi}$, we use the PSO to optimize the antenna position.

A. Performance Optimization Under Fixed Antenna Position

Given the antenna positions, the primary problem is reduced into

$$\begin{aligned}(\text{P2}): \max_{\mathbf{w}_c,\mathbf{R}_r,\mathbf{\Phi}} \quad & R_{sec}(\mathbf{w}_c,\mathbf{R}_r,\mathbf{\Phi}) \\ \text{s.t.} \quad & \mathbf{h}_e^H(\mathbf{w}_c\mathbf{w}_c^H+\mathbf{R}_r)\mathbf{h}_e, \geq \varepsilon, && \text{(14a)} \\ & \|\mathbf{w}_c\|^2+\text{Tr}(\mathbf{R}_r)\leq P_{\max}, && \text{(14b)} \\ & \mathbf{R}_r\succeq \mathbf{0}, && \text{(14c)} \\ & \mathbf{\Phi}=\text{diag}(e^{j\vartheta_1},\ldots,e^{j\vartheta_N}). && \text{(14d)}\end{aligned}$$

This problem is still non-convex. To handle it, we decompose problem (P2) into two sub-problems, namely the joint optimization problem of the communication beamforming and the sensing covariance matrix, and the IRS phase-shift design problem. For the first sub-problem, we adopt a hybrid approach combining SCA and SDR. Specifically, we apply SDR to transform the non-convex problem into a tractable problem. The SDR algorithm relaxes non-convex quadratic optimization problems by replacing the rank-one constraint with positive semidefinite constraints, yielding both a lower bound on the optimal value and approximate solutions via techniques like Gaussian randomization. Then, we use a rank-one reconstruction method to enforce the rank constraint approximately, ensuring the solution quality. For the second sub-problem, we employ a similar SCA-SDR framework. However, due to the limitations of the traditional Gaussian randomization in recovering rank-one solutions, we leverage the successive rank-constrained relaxation (SRCR) algorithm, which iteratively refines solutions while respecting the rank constraint.

1) Optimization of Beamforming Vector and Radar Covariance: Under any given $\mathbf{t}$, $\mathbf{\Phi}$, we define $\mathbf{W}_c=\mathbf{w}_c\mathbf{w}_c^H$, $\mathbf{W}_c\succeq\mathbf{0}$ and $\text{rank}(\mathbf{W}_c)=1$, as well as $\hat{\mathbf{H}}_e=\mathbf{h}_e\mathbf{h}_e^H$ and $\hat{\mathbf{H}}_b=\mathbf{h}_b\mathbf{h}_b^H$. Thus, it has

$$R_b(\mathbf{w}_c,\mathbf{R}_r)=\log_2\left(1+\frac{\text{tr}(\hat{\mathbf{H}}_b\mathbf{W}_c)}{\text{tr}(\hat{\mathbf{H}}_b\mathbf{R}_r)+\sigma^2}\right), \tag{15}$$

$$R_e(\mathbf{w}_c,\mathbf{R}_r)=\log_2\left(1+\frac{\text{tr}(\hat{\mathbf{H}}_e\mathbf{W}_c)}{\text{tr}(\hat{\mathbf{H}}_e\mathbf{R}_r)+\sigma^2}\right), \tag{16}$$

$$\mathcal{P}(\mathbf{w}_c,\mathbf{R}_r,\mathbf{\Phi})=\mathbf{h}_e^H(\mathbf{w}_c\mathbf{w}_c^H+\mathbf{R}_r)\mathbf{h}_e=\text{Tr}\Big(\hat{\mathbf{H}}_e(\mathbf{W}_c+\mathbf{R}_r)\Big). \tag{17}$$

Hence, problem (P2) can be equivalently reformulated as

$$\begin{aligned}(\text{P2.1}): \max_{\mathbf{w}_c,\mathbf{R}_r} \quad & R_b(\mathbf{w}_c,\mathbf{R}_r)-R_e(\mathbf{w}_c,\mathbf{R}_r) \\ \text{s.t.} \quad & \text{tr}\left(\hat{\mathbf{H}}_e(\mathbf{W}_c+\mathbf{R}_r)\right)\geq\varepsilon, && \text{(18a)} \\ & \text{tr}(\mathbf{W}_c)+\text{tr}(\mathbf{R}_r)\leq P_{\max}, && \text{(18b)} \\ & \mathbf{R}_r\geq 0,\mathbf{W}_c\geq 0, && \text{(18c)} \\ & \text{rank}(\mathbf{W}_c)=1. && \text{(18d)}\end{aligned}$$

Note that problem (P2.1) is still non-convex due to the non-convex objective term. To deal with it, we recast the function $R_b(\mathbf{W}_c,\mathbf{R}_r)$ in a form of difference of convex functions, i.e.,

$$R_b(\mathbf{W}_c,\mathbf{R}_r)=F_1(\mathbf{W}_c,\mathbf{R}_r)-F_2(\mathbf{R}_r), \tag{19}$$

where

$$F_1(\mathbf{W}_c,\mathbf{R}_r)=\log_2\left(\sigma^2+\text{tr}(\hat{\mathbf{H}}_b(\mathbf{W}_c+\mathbf{R}_r))\right), \tag{20}$$

$$F_2(\mathbf{R}_r)=\log_2\left(\sigma^2+\text{tr}(\hat{\mathbf{H}}_b\mathbf{R}_r)\right). \tag{21}$$

Similarly, we rewrite the eavesdropping rate as

$$R_e(\mathbf{W}_c,\mathbf{R}_r)=f_1(\mathbf{W}_c,\mathbf{R}_r)-f_2(\mathbf{R}_r), \tag{22}$$

where

$$f_1(\mathbf{W}_c,\mathbf{R}_r)=\log_2\left(\sigma^2+\text{Tr}(\hat{\mathbf{H}}_e(\mathbf{W}_c+\mathbf{R}_r)\right), \tag{23}$$

and

$$f_2(\mathbf{R}_r)=\log_2\left(\sigma^2+\text{Tr}(\hat{\mathbf{H}}_e\mathbf{R}_r)\right). \tag{24}$$

Due to the non-convexity of the objective function, we adopt the SCA technique combining it with the classical majorization-minimization (MM) algorithm to find a concave surrogate function for the objective function, and then solve the problem alternately using this surrogate function. Specifically, the SCA takes advantage of the ease of solving convex optimization problems, transforms non-convex problems into a series of convex subproblems, and obtains an approximated solution to the original problem by alternately solving these subproblems. Hence, by taking the first-order Taylor expansion on the concave function $F_2(\mathbf{R}_r)$ and $f_1(\mathbf{W}_c,\mathbf{R}_r)$, we have

$$\begin{aligned}F_2(\mathbf{R}_r)&\leq F_2(\mathbf{R}_r^{(k_1)})+\text{tr}\left(\frac{1}{\ln 2}\frac{\hat{\mathbf{H}}_b(\mathbf{R}_r-\mathbf{R}_r^{(k_1)})}{\sigma^2+\text{Tr}(\hat{\mathbf{H}}_b\mathbf{R}_r^{(k_1)})}\right) \\ &\triangleq \bar{F}_2(\mathbf{R}_r),\end{aligned} \tag{25}$$

and

$$\begin{aligned}f_1(\mathbf{W}_c,\mathbf{R}_r)&\leq f_1(\mathbf{W}_c^{(k_1)},\mathbf{R}_r^{(k_1)}) \\ &\quad+\text{Tr}\Big(\nabla_{\mathbf{W}_c}^H f_1(\mathbf{W}_c^{(k_1)},\mathbf{R}_r^{(k_1)})(\mathbf{W}_c-\mathbf{W}_c^{(k_1)})\Big) \\ &\quad+\text{Tr}\Big(\nabla_{\mathbf{R}_r}^H f_1(\mathbf{W}_c^{(k_1)},\mathbf{R}_r^{(k_1)})(\mathbf{R}_r-\mathbf{R}_r^{(k_1)})\Big) \\ &\triangleq \bar{f}_1(\mathbf{W}_c,\mathbf{R}_r),\end{aligned} \tag{26}$$

where $\mathbf{W}_c^{(k_1)}$ and $\mathbf{R}_r^{(k_1)}$ are the updates of $\mathbf{W}_c$ and $\mathbf{R}_r$ in the k_1-th iteration, and

$$\begin{aligned}\nabla_{\mathbf{W}_c}^H f_1(\mathbf{W}_c^{(k_1)},\mathbf{R}_r^{(k_1)})&=\nabla_{\mathbf{R}_r}^H f_1(\mathbf{W}_c^{(k_1)},\mathbf{R}_r^{(k_1)}) \\ &=\frac{1}{\ln 2}\frac{\hat{\mathbf{H}}_e}{\sigma^2+\text{Tr}\left(\hat{\mathbf{H}}_e\mathbf{W}_c^{(k_1)}+\text{Tr}(\hat{\mathbf{H}}_e\mathbf{R}_r^{(k_1)})\right)}.\end{aligned} \tag{27}$$

Utilizing (25) and (26), we construct a lower bound function for the objective function of problem (P2.1), and serve it as the surrogate function. Consequently, problem (P2.1) can be approximated as

$$(\text{P2.2}) \max_{\mathbf{W}_c,\mathbf{R}_r} F_1(\mathbf{W}_c,\mathbf{R}_r)-\bar{F}_2(\mathbf{R}_r)$$

$$- \bar{f}_1(\mathbf{W}_c, \mathbf{R}_r) + f_2(\mathbf{R}_r)$$
$$\text{s.t.} \quad (18a),\ (18b),\ (18c),\ (18d).$$

Using the SDR method to remove the rank constraint (18d), the transmit beamforming subproblem can be transformed as

$$(\text{P2.3}) \max_{\mathbf{W}_c, \mathbf{R}_r} F_1(\mathbf{W}_c, \mathbf{R}_r) - \bar{F}_2(\mathbf{R}_r) - \bar{f}_1(\mathbf{W}_c, \mathbf{R}_r) + f_2(\mathbf{R}_r)$$
$$\text{s.t.} \quad (18a),\ (18b),\ (18c),$$

which is a convex problem and can be solved by CVX. Let $\mathbf{W}_c^\star$ and $\mathbf{R}_r^\star$ represent the optimal solution obtained to problem (P2.3). However, due to the lack of the rank-one constraint, the obtained solution may not be optimal to problem (P2.2). Therefore, according to [66], it is necessary to construct a solution that satisfies the rank-one constraint, as given in the following lemma.

Lemma 1: Given the optimal solution $\mathbf{W}_c^\star$ and $\mathbf{R}_r^\star$ to problem (P2.3), the optimal solution to problem (P2.2) is

$$\mathbf{w}_c^{opt} = \left(\mathbf{h}_e^H \mathbf{W}_c^\star \mathbf{h}_e\right)^{-1/2} \mathbf{W}_c^\star \mathbf{h}_e, \tag{28}$$

$$\mathbf{R}_r^{opt} = \mathbf{R}_r^\star + \mathbf{W}_c^\star - \mathbf{w}_c^{opt} \left(\mathbf{w}_c^{opt}\right)^H. \tag{29}$$

Proof: Define $\mathbf{W}_c^{opt} = \mathbf{w}_c^{opt}(\mathbf{w}_c^{opt})^H \succeq 0$ (of rank one), and $\mathbf{R}_r^{opt}$ are the optimal solutions to problem (P2.1). According to (29), $\mathbf{W}_c^{opt} + \mathbf{R}_r^{opt} = \mathbf{W}_c^\star + \mathbf{R}_r^\star$. Thus, it satisfies the power constraint of the objective. It is not difficult to prove $\text{tr}(\hat{\mathbf{H}}_e(\mathbf{W}_c^{opt} + \mathbf{R}_r^{opt})) = \text{tr}(\hat{\mathbf{H}}_e(\mathbf{W}_c^\star + \mathbf{R}_r^\star))$, so it meets the sensing performance index of the objective. Therefore, it completes the proof.

The detailed algorithm for solving $\mathbf{w}_c$ and $\mathbf{R}_r$ is summarized in Algorithm 1. Here, ϵ_1 represents the precision of convergence. In the initialization phase, the maximum transmission criterion (MRT) is adopted. The phase shift matrix $\mathbf{\Phi}^{(0)}$ is set as an identity matrix. On this basis, in accordance with the MRT criterion and following the principle that the beam direction is consistent with the equivalent channel direction, the beamforming vector is precisely aligned with the user and target directions. Through this method, the useful signal can be maximally enhanced in the initial state, thereby obtaining the parameters $\mathbf{w}_c^{(0)}$ and $\mathbf{R}_r^{(0)}$ in the initial state.

2) Optimization of Phase Shift of IRS: With $\mathbf{w}_c$ and $\mathbf{R}_r$ according to Algorithm 1, we define $\mathbf{v} = (e^{j\vartheta_1}, e^{j\vartheta_2}, \ldots, e^{j\vartheta_N})^H$. Then, we introduce the following relationships. First, consider $\boldsymbol{\zeta}_i^H \mathbf{w}_c = \mathbf{v}\,\text{diag}(\boldsymbol{\zeta}_i^H)\mathbf{H}(\mathbf{t})^H \mathbf{w}_c$, where $i \in (b, e)$. By introducing $\mathbf{V} = \mathbf{v}\mathbf{v}^H$, we can obtain $|\boldsymbol{\zeta}_i^H \mathbf{w}_c|^2 \triangleq \text{Tr}(\hat{\mathbf{A}}_i \mathbf{V})$. Here, $\hat{\mathbf{A}}_i = \text{diag}(\boldsymbol{\zeta}_i)^H \mathbf{H}^H \mathbf{w}_c \mathbf{w}_c^H \mathbf{H}\,\text{diag}(\boldsymbol{\zeta}_i)$ and $i \in (b, e)$. Similarly, for $\boldsymbol{\zeta}_i^H \mathbf{R}_r \boldsymbol{\zeta}_i$, we have $\boldsymbol{\zeta}_i^H \mathbf{R}_r \boldsymbol{\zeta}_i = \text{Tr}(\hat{\mathbf{N}}_i \mathbf{V})$, with $\hat{\mathbf{N}}_i = \text{diag}(\boldsymbol{\zeta}_i)^H \mathbf{H}^H \mathbf{R}_r^H \mathbf{H}\,\text{diag}(\boldsymbol{\zeta}_i)$ and $i \in (b, e)$. Thus, the optimization problem can be expressed as

$$(\text{P2.4}): \max_{\mathbf{V}} \log_2\left(1 + \frac{\text{Tr}(\hat{\mathbf{A}}_b \mathbf{V})}{\text{Tr}(\hat{\mathbf{N}}_b \mathbf{V}) + \sigma^2}\right) - \log_2\left(1 + \frac{\text{Tr}(\hat{\mathbf{A}}_e \mathbf{V})}{\text{Tr}(\hat{\mathbf{N}}_e \mathbf{V}) + \sigma^2}\right)$$

Algorithm 1: SCA-based algorithm for solving problem (P2.1).

Input: $\{\mathbf{w}_c^{(0)}, \mathbf{R}_r^{(0)}\}$.
Initialize $\Delta = \infty$, $k_1 = 0$;
While $(\Delta \geq \epsilon_1)$
At the k_1-th iteration, solve the non-convex problem (P2.3) and get $\mathbf{W}_c^\star$ and $\mathbf{R}_r^\star$;
Construct $\mathbf{w}_c^{opt}$ and $\mathbf{R}_r^{opt}$ using equations (28) and (29) for the (k_1+1)-th iteration to get $\mathbf{W}_c^{(k_1+1)}$ and $\mathbf{R}_r^{(k_1+1)}$;
Calculate $R_{sec}^{(k_1+1)}$ based on $\mathbf{w}_c^{opt}$ and $\mathbf{R}_r^{opt}$;
Update
$\Delta = |R_{sec}^{(k_1+1)} - R_{sec}^{(k_1)}|$, $R_{sec}^{(k_1)} \leftarrow R_{sec}^{(k_1+1)}$;
$\mathbf{w}_c^{k_1} = \mathbf{w}_c^{opt}$, $\mathbf{R}_r^{k_1} = \mathbf{R}_r^{opt}$, $k_1 = k_1 + 1$;
End while
Output: $\{\mathbf{w}_c^{opt}, \mathbf{R}_r^{opt}\}$.

$$\text{s.t.} \quad \text{Tr}(\hat{\mathbf{N}}_e \mathbf{V}) \geq \varepsilon, \tag{30a}$$
$$\mathbf{V} \succeq 0, \tag{30b}$$
$$\text{rank}(\mathbf{V}) = 1, \tag{30c}$$
$$[\mathbf{V}]_{n,n} = 1, \quad n \in \mathcal{N}. \tag{30d}$$

According to the properties of logarithms, the objective function can be transformed into

$$R_{sec}(\mathbf{V}) = \log_2\left(\sigma^2 + \text{Tr}(\hat{\mathbf{N}}_b \mathbf{V}) + \text{Tr}(\hat{\mathbf{A}}_b \mathbf{V})\right) \underbrace{- \log_2\left(\sigma^2 + \text{Tr}(\hat{\mathbf{N}}_b \mathbf{V})\right)}_{I_1(\mathbf{V})} \underbrace{- \log_2\left(\sigma^2 + \text{tr}(\hat{\mathbf{A}}_e \mathbf{V}) + \text{tr}(\hat{\mathbf{N}}_e \mathbf{V})\right)}_{I_2(\mathbf{V})} + \log_2\left(\sigma^2 + \text{Tr}(\hat{\mathbf{N}}_e \mathbf{V})\right). \tag{31}$$

By leveraging the SCA approach to approximate its convexity, we check its first-order Taylor expansion on I_1 (V) and I_2 (V) to obtain their upper bounds, which can be expressed as

$$I_1(\mathbf{V}) \leq \log_2\left(\sigma^2 + \text{tr}(\hat{\mathbf{N}}_b \mathbf{V}^{(k_2)})\right) + \text{Tr}\left(\frac{1}{\ln 2} \frac{\hat{\mathbf{N}}_b}{\sigma^2 + \text{tr}(\hat{\mathbf{N}}_b \mathbf{V}^{(k_2)})} (\mathbf{V} - \mathbf{V}^{(k_2)})\right), \tag{32}$$

and

$$I_2(\mathbf{V}) \leq \log_2\left(\sigma^2 + \text{tr}(\hat{\mathbf{A}}_e \mathbf{V}^{(k_2)}) + \text{tr}(\hat{\mathbf{N}}_e \mathbf{V}^{(k_2)})\right) + \text{Tr}\left(\frac{1}{\ln 2} \frac{\hat{\mathbf{N}}_e + \hat{\mathbf{A}}_e}{\sigma^2 + \text{tr}(\hat{\mathbf{N}}_e \mathbf{V}^{(k_2)}) + \text{tr}(\hat{\mathbf{A}}_e \mathbf{V}^{(k_2)})} (\mathbf{V} - \mathbf{V}^{(k_2)})\right), \tag{33}$$

where $\mathbf{V}^{(k_2)}$ is the locally optimal solution at the k_2-th iteration. Substituting the upper bounds of $I_1(\mathbf{V})$ and $I_2(\mathbf{V})$ in (32) and (33) and omitting the constant terms in (31), problem (P2.4) can

be reformulated as

$$\begin{aligned}(\text{P2.5}): \max_{\mathbf{V}} \ & \log_2\left(\sigma^2+\text{Tr}(\hat{\mathbf{N}}_b\mathbf{V})+\text{Tr}(\hat{\mathbf{A}}_b\mathbf{V})\right) \\ & -\text{Tr}\left(\frac{1}{\ln 2}\frac{\hat{\mathbf{N}}_b\mathbf{V}}{\sigma^2+\text{tr}(\hat{\mathbf{N}}_b\mathbf{V}^{(k_2)})}\right) \\ & -\text{Tr}\left(\frac{1}{\ln 2}\frac{\hat{\mathbf{N}}_e+\hat{\mathbf{A}}_e}{\sigma^2+\text{tr}(\hat{\mathbf{N}}_e\mathbf{V}^{(k_2)})+\text{tr}(\hat{\mathbf{A}}_e\mathbf{V}^{(k_2)})}\mathbf{V}\right) \\ & +\log_2\left(\sigma^2+\text{Tr}(\hat{\mathbf{N}}_e\mathbf{V})\right) \\ \text{s.t.}\ & \text{(30a)}, \text{(30b)}, \text{(30c)}, \text{(30d)}.\end{aligned}$$

It can be observed that the convex problem can be effectively solved by relaxing the constraint $\text{rank}(\mathbf{V})=1$ in (30c). The SDR and Gaussian randomization algorithm can be used to obtain an approximate solution for $\mathbf{v}$, but it cannot guarantee the convergence of the overall algorithm. SRCR diverges from traditional algorithms, which entirely abandon the rank-one constraint. Instead, it adjusts the constraint condition through the relaxation parameter $\varpi \in [0,1]$. When $\varpi=0$, it's tantamount to discarding the rank-one constraint, allowing for the discovery of a feasible point. As ϖ steadily rises from 0, the rank-one constraint is progressively met until it eventually nears the true rank-one constraint set. Therefore, according to [67], SRCR is adopted to equivalently transform (30c) into

$$\boldsymbol{u}_{\max}^H\left(\mathbf{V}^{(k_2)}\right)\mathbf{V}\boldsymbol{u}_{\max}\left(\mathbf{V}^{(k_2)}\right) \geqslant \varpi^{(k_2)}\text{Tr}\left(\mathbf{V}\right), \tag{34}$$

where $\mathbf{V}^{(k_2)}$ represents a feasible solution obtained at the k_2-th iteration. The eigenvector corresponding to the largest eigenvector of $\mathbf{V}^{(k_2)}$ is denoted as $\boldsymbol{u}_{\max}(\mathbf{V}^{(k_2)})$. Additionally, we sequentially increase $\varpi^{(k_2)}$ from 0 to 1 through iterations in order to gradually approach a rank-one solution. After each iteration, the relaxation parameter can be updated as

$$\varpi^{(k_2+1)} \leftarrow \min\left(1, \frac{\chi_{\max}(\mathbf{V}^{(k_2+1)})}{\text{tr}(\mathbf{V}^{(k_2+1)})}+\varrho^{(k_2+1)}\right), \tag{35}$$

where $\chi_{\max}(\mathbf{V}^{(k_2+1)})$ represents the largest eigenvalue of $\mathbf{V}^{(k_2+1)}$ and $\varrho^{(k_2+1)}$ denotes the step size for the weight parameter updating. The optimization problem can then be expressed

$$\begin{aligned}(\text{P2.6}): \max_{\mathbf{V}} \ & \log_2\left(\sigma^2+\text{Tr}(\hat{\mathbf{N}}_b\mathbf{V})+\text{Tr}(\hat{\mathbf{A}}_b\mathbf{V})\right) \\ & -\text{Tr}\left(\frac{1}{\ln 2}\frac{\hat{\mathbf{N}}_e\mathbf{V}}{\sigma^2+\text{tr}(\hat{\mathbf{N}}_e\mathbf{V}^{(k_2)})}\right) \\ & -\text{Tr}\left(\frac{1}{\ln 2}\frac{(\hat{\mathbf{N}}_e+\hat{\mathbf{A}}_e)\mathbf{V}}{\sigma^2+\text{tr}(\hat{\mathbf{N}}_e\mathbf{V}^{(k_2)})+\text{tr}(\hat{\mathbf{A}}_e\mathbf{V}^{(k_2)})}\right) \\ & +\log_2\left(\sigma^2+\text{Tr}(\hat{\mathbf{N}}_e\mathbf{V})\right) \\ \text{s.t.}\ & \text{(30a)}, \text{(30b)}, \text{(30d)}, \text{(34)}.\end{aligned}$$

Problem (P2.6) can be solved by the CVX tool. Similarly, the detailed algorithm steps for optimizing $\mathbf{V}$ by using the SCA algorithm will be described in Algorithm 2. Here, ϵ_2 represents the predefine threshold and when $\Delta_2=\text{Tr}(\mathbf{V}^{(k_2)})/\chi_{\max}(\mathbf{V}^{(k_2)})$ is less than ϵ_2, the objective value of problem (P2.6) converges. After calculating matrix $\mathbf{V}^\star$ according to Algorithm 2, find the eigenvector $\mathbf{e}^{\text{opt}}$ corresponding to its maximum eigenvalue. Then Φ is the diagonal matrix formed with $\mathbf{e}^{\text{opt}}$ as its diagonal elements.

Algorithm 2: SCA-based algorithm for solving problem (P2.4).

Input: $\{\mathbf{w}_c^{opt}, \mathbf{R}_r^{opt}\}$.
Initialize a feasible iteration point $\{\mathbf{V}^{(0)}\}$, $\varrho^{(0)}$.
Set $\Delta_2=\infty$, $\varpi^{(0)}=0$, $k_2=0$;
While $(\Delta_2 \geq \epsilon_2)$
  Solve non-convex problem (P2.6) with $\{\varpi^{(k_2)}, \mathbf{V}^{(k_2)}\}$ to obtain $\mathbf{V}^\star$;
  IF (problem (P2.6) is solvable)
    Update $\mathbf{V}^{(k_2+1)}=\mathbf{V}^\star$, $\varrho^{(k_2+1)}=\varrho^{(0)}$; **Else**
    Update $\mathbf{V}^{(k_2+1)}=\mathbf{V}^{(k_2)}$, $\varrho^{(k_2+1)}=\frac{\varrho^{(k_2)}}{2}$; **End**
  Update $\varpi^{(k_2+1)}$ by (35) and $k_2=k_2+1$;
  Calculate $\Delta_2=\frac{\text{Tr}(\mathbf{V}^{(k_2)})}{\chi_{\max}(\mathbf{V}^{(k_2)})}$;
Endwhile

B. Optimization of Antenna Position

With the obtained $\mathbf{w}_c$, $\mathbf{R}_r$ and $\mathbf{\Phi}$, we next optimize the antenna position $\mathbf{t}$. Thus, the original problem (P1) can be reduced into the following optimization problem

$$\begin{aligned}(\text{P3}): \max_{\mathbf{t}} \ & R_{sec}(\mathbf{t}) \\ \text{s.t.}\ & \mathbf{h}_{r,e}^H\mathbf{\Phi}\mathbf{H}(\mathbf{t})^H(\mathbf{w}_c\mathbf{w}_c^H+\mathbf{R}_r)\mathbf{H}(\mathbf{t})\mathbf{\Phi}^H\mathbf{h}_{r,e} \geq \varepsilon, && \text{(36a)} \\ & |t_i-t_j| \geq d_{\min}, \forall i,j \in \mathcal{M}, i\neq j, && \text{(36b)} \\ & t_m \in [0,J], \forall m \in \mathcal{M}. && \text{(36c)}\end{aligned}$$

Note that the high non-convexity of the above problem makes it challenging to solve. Moreover, the high-dimensional transmit response matrix of the moving antennas significantly increases the complexity of the problem when using search-based methods. Therefore, the problem can be solved by using the PSO algorithm.

Specifically, the principle of PSO lies in representing each potential solution within the solution space by a particle. These particles fly at a certain speed. During the flight, they adjust their positions continuously based on their respective personal best positions and the global best position found by the entire particle swarm, constantly searching for the global optimal solution. We first introduce S particles and initialize their positions and velocities to $\mathbf{P}=\{\boldsymbol{p}_1^{(0)}, \boldsymbol{p}_1^{(0)}, \ldots, \boldsymbol{p}_S^{(0)}\}$ and $\mathbf{U}=\{\boldsymbol{\mu}_1^{(0)}, \boldsymbol{\mu}_2^{(0)}, \ldots, \boldsymbol{\mu}_S^{(0)}\}$, respectively, where $\mu_s^{(0)}$ represents the initial velocity of particle s and each particle represents a possible solution for antenna position, i.e.,

$$\boldsymbol{p}_s^{(0)}=[t_{s,1}^{(0)}, t_{s,2}^{(0)}, \ldots, t_{s,M}^{(0)}], \tag{37}$$

where $0 \leq t_{s,k}^{(0)} \leq J$ for $1 \leq k \leq M, 1 \leq k \leq S$, which represents the possible position of the k-th antenna of the s-th particle

within the finite movement region. The PSO algorithm could efficiently search for the optimal particle among these S particles and identify it as the solution to problem (P3). The detailed process is outlined as follows.

1) Definition of the Fitness Function: The fitness function is used to evaluate the performance of each particle, which means to determine whether the particle's position can achieve the desired performance requirements. Considering constraints (13a) and (13e), we introduce a penalty function as

$$\mathcal{I}\left(\boldsymbol{p}_s^{(q)}\right) = \tau_t \sum_{a=1}^{M-1} \sum_{\tilde{a}=a+1}^{M} \delta\left(\left|t_a^{(q)} - t_{\tilde{a}}^{(q)}\right| < d_{\min}\right) + \tau_r \delta\left(\mathcal{P}\left(\boldsymbol{p}_s^{(q)}\right) < \epsilon\right), \forall s \in [1, S], \tag{38}$$

where $\boldsymbol{p}_s^{(q)}$ is the antenna position of the s-th particle in the q-th $(1 \le q \le Q)$ iteration, and Q denotes the maximum number of iterations. τ_t and τ_r represent the penalty factors for the antenna position constraint (13e) and the sensing constraint (13a), respectively. They can adjust the severity of the penalties. $\delta(\cdot)$ is an indicator function, which equals 1 when the condition is satisfied and 0 otherwise. Thus, the fitness function is defined as

$$\mathcal{F}\left(\boldsymbol{p}_s^{(q)}\right) = R_{sec}\left(\boldsymbol{p}_s^{(q)}\right) - \mathcal{I}\left(\boldsymbol{p}_s^{(q)}\right). \tag{39}$$

At the same time, τ_t and τ_r need to use the penalty function at position $R_{sec}(\boldsymbol{p}_s^{(q)}) - (\tau_{\mathrm{t}} + \tau_{\mathrm{r}}) < 0$ to drive the particles to satisfy the relevant constraints. Therefore, as the number of iterations increases, the penalty function $\mathcal{I}(\boldsymbol{p}_s^{(q)})$ will converge to 0.

2) Updating of the Particles' Positions and Pelocities: The position of the s-th particle is controlled by its own local best position $\boldsymbol{p}_s^{\star}$ and the global best position $\boldsymbol{p}^{\star}$ among all particles, which is evaluated by the fitness function. Therefore, according to [68], the position and velocity update of the s-th particle can be expressed as

$$\begin{aligned} &\boldsymbol{v}_s^{(q+1)} = \varsigma \boldsymbol{v}_s^{(q)} + c_1 r_2 (\boldsymbol{p}_s^{\star} - \boldsymbol{p}_s^{(q)}) + c_2 r_3 (\boldsymbol{p}^{\star} - \boldsymbol{p}_s^{(q)}), \\ &s = 1, \ldots, S, p_s^{(q+1)} = \mathcal{B}\left(\boldsymbol{p}_s^{(q)} + \boldsymbol{v}_s^{(q+1)}\right), \end{aligned} \tag{40}$$

where c_1 and c_2 are individual and global learning factors, respectively, for determining the step size of each particle moving towards the best position; r_2 and r_3 are two random parameters uniformly distributed in [0,1], which aim to increase the randomness of the search for escaping from local optima; ς represents the inertia weight, to balances the particle's search speed and accuracy [68], its value will gradually decrease as the number of iterations increases, which is shown as

$$\varsigma = \left(\varsigma_{\max} - \frac{(\varsigma_{\max} - \varsigma_{\min})}{Q} q\right), \tag{41}$$

where $\varsigma_{\max}$ and $\varsigma_{\min}$ are the maximum and minimum value of ς.

Since the antenna position cannot exceed the movement range, namely constraint (13f), the coordinates of points that exceed the range are mapped to the corresponding maximum/minimum values,

$$[\mathcal{B}(\tilde{\boldsymbol{p}})]_i = \begin{cases} 0, & \text{if } [\tilde{\boldsymbol{p}}]_i < 0, \\ J, & \text{if } [\tilde{\boldsymbol{p}}]_i > J, \\ [\tilde{\boldsymbol{p}}]_i, & \text{otherwise.} \end{cases} \tag{42}$$

Therefore, according to the mapping function $\mathcal{B}(\tilde{\boldsymbol{p}})$, it ensures that the antenna position remains within the feasible region throughout the iteration process.

C. Overall Solution

The overall algorithm framework proceeds as follows. Initially, S particles are initialized with randomized positions and velocities under predefined system constraints. For each particle's antenna configuration, the variables of transmit beamforming $\mathbf{w}_c$, sensing covariance matrix $\mathbf{R}_r$ and IRS phase shifts $\boldsymbol{\Phi}$ are iteratively optimized via Algorithm 1 and Algorithm 2, with the corresponding secure rate R_{sec} serving as the fitness metric. Following this, local best positions $\mathbf{p}_s^{\star}$ and the global best $\mathbf{p}^{\star}$ are updated through fitness comparisons. During Q iterations, the inertia weight ς is dynamically scaled, after which velocity and position vectors are refreshed using PSO kinematic rules. Each update triggers re-evaluation of R_{sec}, $\mathbf{p}_s^{\star}$ and $\mathbf{p}^{\star}$. Upon convergence, the optimal antenna configuration $\mathbf{t}$ is derived from $\mathbf{p}^{\star}$, yielding the joint solutions $\mathbf{w}_c$, $\mathbf{R}_r$ and $\boldsymbol{\Phi}$ that satisfy all security and sensing constraints. The overall algorithm details for solving problem (P1) are summarized in Algorithm 3.

IV. Numerical Results

In this section, we present numerical simulation results to demonstrate the performance of the algorithm. We consider the distance-dependent path loss model, that is, $\beta = \beta_0 (d/d_0)^{-\overline{\alpha}}$, where $\beta_0 = -30$ dB represents the path loss at the reference distance of $d_0 = 1$ m, and we set $\overline{\alpha}$ as 2.2. Throughout the simulation, we set the positions of the BS and IRS as (0 m, 0 m), (0 m, 50 m). The user and target are placed 2 m away from the IRS, with the azimuth angles of both the user and the target relative to the IRS set to $\pi/6$ and $-\pi/6$, Additionally, some parameters are carefully defined in Table II.

It is observed from Fig. 2(a), regardless of how the parameters are set, the proposed algorithm can achieve convergence in a consistent way. Further observation reveals that when other parameters remain unchanged, there are obvious correlations between the secure rate and the number of antennas, the number of IRS, the movement range of antennas, and the sensing threshold. Specifically, as the number of antennas increases, the secure rate may increase accordingly; changes in the number of IRS also have an impact on the secure rate; the size of the antenna movement range affects the change of the secure rate to a certain extent; and the adjustment of the sensing threshold also shows a certain correlation with the secure rate.

Fig. 2(b) performs a comparative analysis of the performance between the FPA and the MA. The results show that the performance of both can gradually converge as the number of iterations increases. However, compared to the FPA, the MA demonstrates

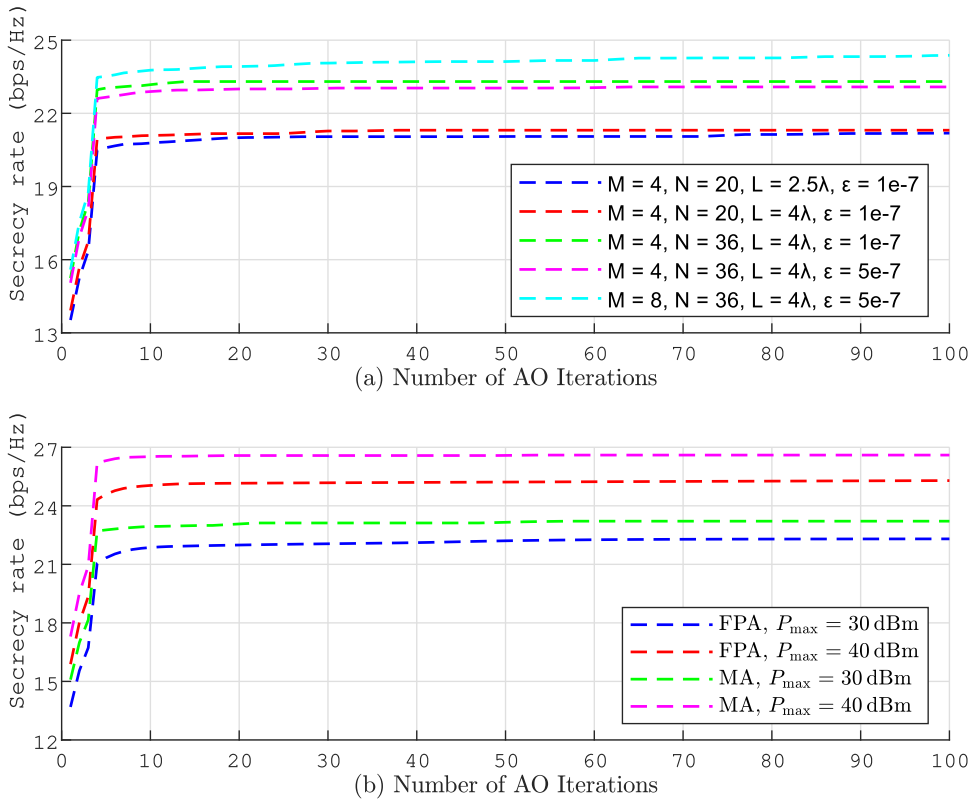

Fig. 2. Convergence performance of the proposed algorithm.

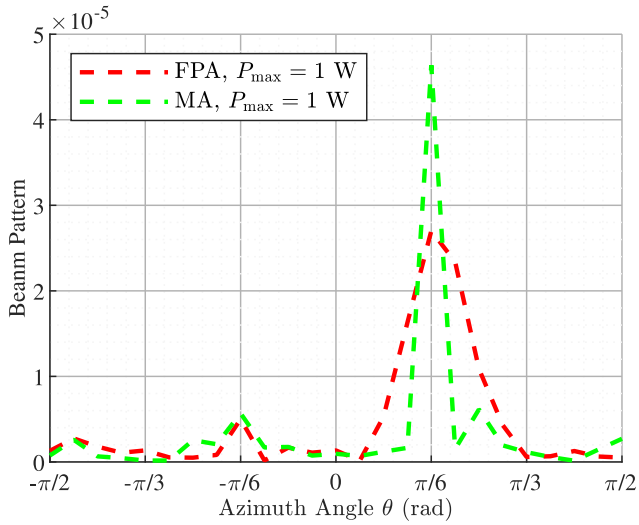

Fig. 3. Beam gain diagram.

significant advantages and can achieve a higher communication security rate. This result strongly proves the important role of the MA in channel reconstruction. It can better adapt to changes in the channel environment by flexible position adjustment, thereby enhancing the security and efficiency of communication.

Fig. 3 clearly presents the beam gain of the signal. Through careful observation of this figure, it can be found that when certain specific conditions are met, the signal strength reaches its peak, which fully indicates that the signal power is maximized in the direction of the user. In the direction of the eavesdropping target, the signal also has a certain power. During the simulation, the sensing threshold is set at 5 μW, and at this time, the signal strength can exactly reach this threshold level, which means that the minimum requirement for sensing performance is met. In short, this result shows that during the process of exploring the target, the goal of enabling the user to obtain the strongest energy has been successfully achieved. While ensuring the sensing performance, the signal power distribution in the user's direction has been optimized.

Three benchmark algorithms are introduced for comparison with the proposed algorithm.

- *FPA:* This ignores the optimization of antenna positions and selects a traditional fixed-position antenna array. It jointly optimizes the IRS phase shifts, communication beamforming, and the sensing covariance matrix.
- *Fixed IRS:* It indicates ignoring the optimization of IRS phase shifts, selecting fixed IRS phase shifts, and only optimizing the antenna positions, communication beamforming, and the sensing covariance matrix.
- *Zero-forcing (ZF):* Both communication beamforming and the sensing covariance are solved using ZF approach, and it jointly optimizes IRS phase shifts and antenna positions.

In Fig. 4, the inherent relationship between the transmit power and the secure rate is depicted. Through careful observation of the data in the figure, it can be found that as the transmit power gradually increases, the secure rate shows a clear linear growth trend. This phenomenon indicates that, in the current research context, an increase in transmit power can effectively

Algorithm 3: PSO-based algorithm for solving problem (P1).

N, M, J, σ^2, ϵ_1, ϵ_2, d_r, ε, $d_{\min}$, $P_{\max}$, Q, $\varsigma_{\max}$, $\varsigma_{\min}$, c_1, c_2, τ_t, τ_r, $\{\theta_{m,l}\}$, $\{\rho_r^l(\mathbf{r}_n)\}$.
Initialize the velocity $\mathbf{U}^{(0)}$ and position $\mathbf{P}^{(0)}$ of S particles;
Based on the initial positions of the particles, combined with Algorithm 1 and Algorithm 2, solve for the corresponding values of $\mathbf{w}_c^{(0)}$, $\mathbf{R}_r^{(0)}$, $\mathbf{V}^{(0)}$, and calculate $R_{sec}^{(0)}$. Set $R_{sec}(\boldsymbol{p}_n^{(0)}) = R_{sec}^{(0)}$, and then calculate the fitness value for each particle according to (39);
Let the local best position $\boldsymbol{p}_s^\star = \boldsymbol{p}_s^{(0)}$, and the global best position
$\boldsymbol{p}^\star = \arg\max_{\boldsymbol{p}_n^{(0)}} \{\mathcal{F}(\boldsymbol{p}_1^{(0)}), \mathcal{F}(\boldsymbol{p}_2^{(0)}), \ldots, \mathcal{F}(\boldsymbol{p}_S^{(0)})\}$;
For ($q = 1$ to Q)
  Calculate ς according to (41);
  For (s = 1 to S)
    Update the positions and velocities of the particles respectively according to (40) and (40);
    Evaluate the fitness function of particle s by combining with Algorithm 1 and Algorithm 2, and then update it;
    If $(\mathcal{F}(\boldsymbol{p}_s^{(q)}) > \mathcal{F}(\boldsymbol{p}_{s,best}))$
      Update $\boldsymbol{p}_{s,best} = \boldsymbol{p}_s^{(q)}$;
    Else
    If $(\mathcal{F}(\boldsymbol{p}_s^{(q)}) > \mathcal{F}(\boldsymbol{p}_{best}))$
      Update $\boldsymbol{p}_{best} = \boldsymbol{p}_s^{(q)}$;
    End
  End
End
Obtain $\mathbf{t} = \boldsymbol{p}_{best}$;
Calculate the corresponding $\mathbf{w}_c$, $\mathbf{R}_r$ and $\boldsymbol{\Phi}$ according to Algorithm 1 and Algorithm 2.

drive an increase in the secure rate. Meanwhile, it is particularly noteworthy that the proposed scheme significantly outperforms the other three comparative schemes in terms of performance. Whether in the stage of lower transmit power or when the transmit power is relatively high, the secure rate corresponding to this scheme always remains at a higher level. This not only fully demonstrates the effectiveness and superiority of the scheme proposed in this paper but also further illustrates that the reasonable setting of various variables has a positive promoting effect on the improvement of the secure rate.

Fig. 5 mainly presents the relationship between the number of IRS reflection elements and the secure rate. It is not difficult to find from the figure that as the number of IRS reflection elements gradually increases, the security rate has been significantly improved, showing a favorable increasing trend. This clearly indicates that the IRS has a positive feedback effect on the performance of ISAC. More IRS reflection elements can optimize the signal propagation path and enhance the signal strength, thereby improving the system's secure rate, highlighting the key value of the IRS in improving the performance of ISAC. It is worth

TABLE II
SIMULATION PARAMETERS

Parameter	Description	Value
M	Number of antennas	4
N	Number of IRS elements	36
J	The length of the linear transmit array	4λ
d_{min}	Minimum inter-MA distance	$\lambda/2$
L	Number of channel paths	10
ρ_0	Path loss at the reference distance	-30 dB
α	Path loss exponent	2.2
σ^2	Average noise powers	-110 dBm
$P_{\max}$	Power of ISAC BS	10 dBm
S	Number of particles	100
Q	Maximum numbers of iterations	100
τ_t	Penalty factors for antenna position	10
τ_r	Penalty factors for sensing constraint	10
c_1	Personal learning factors	1.4
c_2	Global learning factors	1.4
ϵ_1	Convergence thresholds for beamforming	10^{-4}
ϵ_2	Convergence thresholds for $\boldsymbol{\Phi}$	10^{-4}

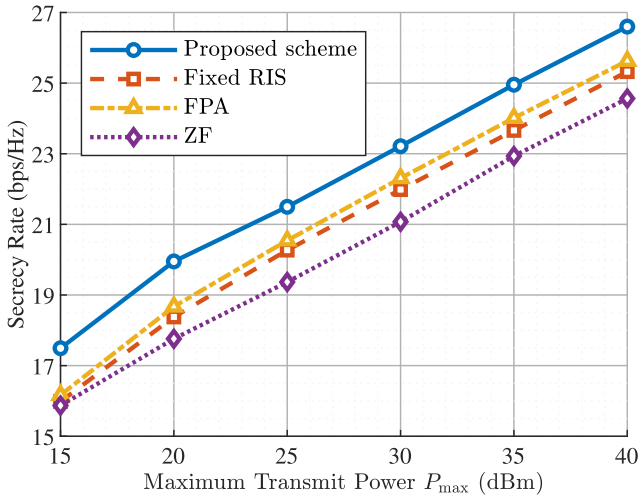

Fig. 4. Secure rate R_{sec} versus transmission power.

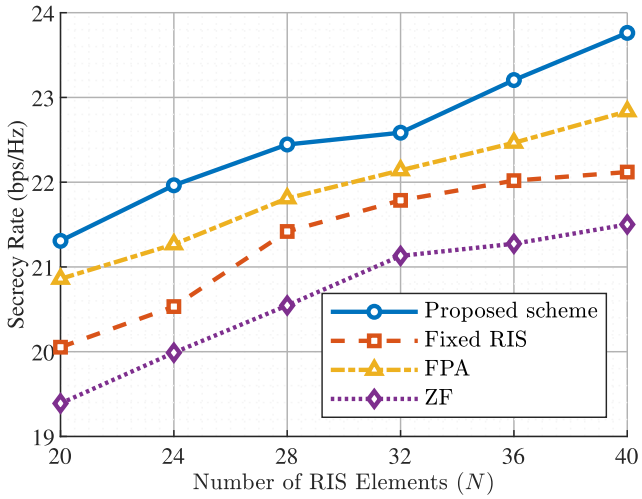

Fig. 5. Secure rate R_{sec} versus Number os IRS elements.

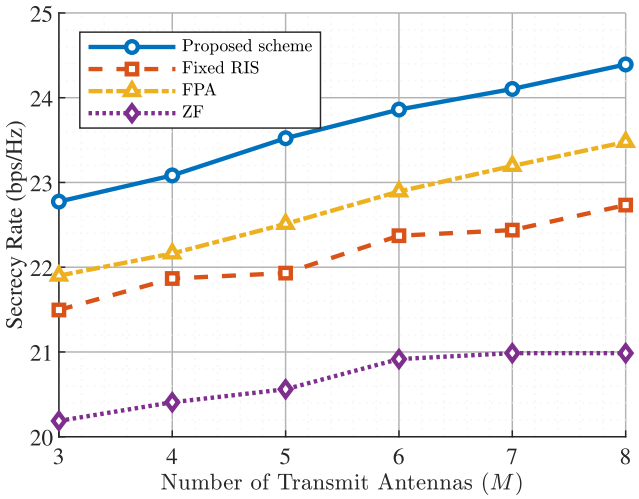

Fig. 6. Secure rate R_{sec} versus number of transmit antennas.

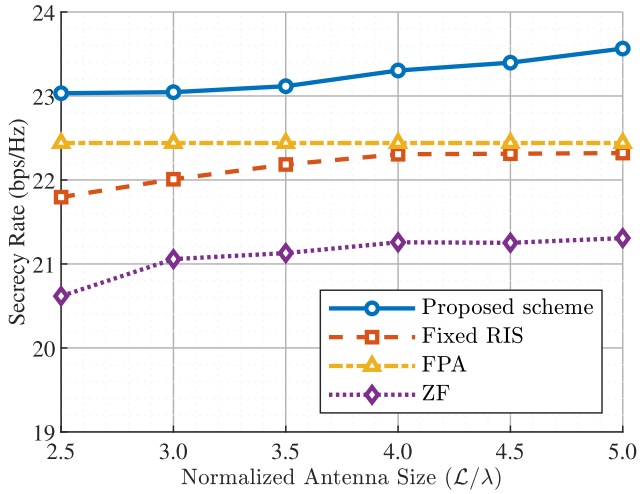

Fig. 8. Secure rate R_{sec} versus normalized antenna size.

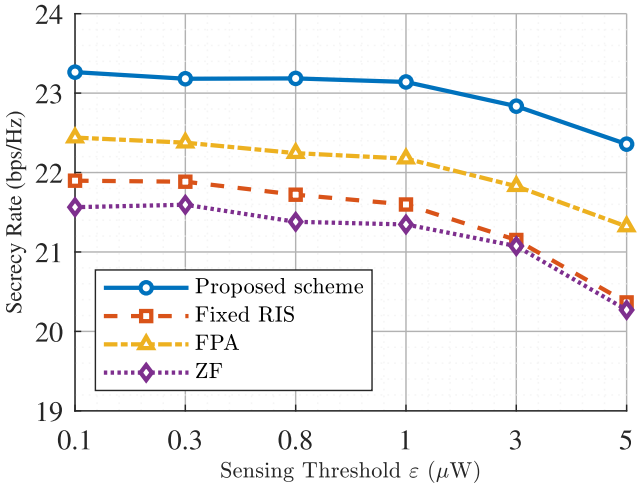

Fig. 7. Secure rate R_{sec} versus sensing beamforming gain.

noting that under the same conditions, the proposed algorithm could perform better in improving the secure rate compared with other benchmarking schemes.

Fig. 6 reveals the close relationship between the secure rate and the number of BS transmitting antennas. It can be intuitively and obviously observed from the figure that as the number of BS transmitting antennas gradually increases, the secure rate shows a significant upward trend and achieves a relatively large increase. This phenomenon fully demonstrates that expanding the scale of antennas has an extremely favorable promoting effect on improving the performance of wireless communication. It means that in a wireless communication system, increasing the number of BS transmitting antennas can effectively enhance the stability and efficiency of signal transmission, laying a solid foundation for the improvement of the secure rate.

Fig. 7 shows the impact of the sensing threshold on secure communication performance. As shown in the figure, as the sensing threshold increases, the security performance declines. At the sensing threshold of $\varepsilon = 0.8\ \mu W$, the proposed scheme outperforms the fixed RIS by 0.28 dB, the FPA by 0.18 dB, and the ZF by 0.35 dB in secrecy rate, as clearly indicated by the visual annotations. This is mainly due to the trade-off between sensing and communication. When sensing performance improves (i.e., when more energy is directed towards eavesdropper detection), the signal strength available for legitimate users weakens. As the sensing performance constraints are further tightened, the security performance will drop sharply. This is because enhanced sensing performance leads to improved signal quality at the eavesdropping target, thereby exacerbating the degradation of security performance. Identifying the optimal trade-off between sensing and security remains a significant challenge.

Fig. 8 illustrates the relationship between the normalized antenna size ($\mathcal{L}/\lambda$) and the secrecy rate. Since the FPA antenna is a fixed antenna, its performance remains unaffected and stays as a straight line with the increase in the normalized size of the antenna. As the normalized antenna size increases, the proposed scheme can leverage more spatial channel information, leading to a continuous improvement in the secrecy rate. When the normalized antenna size reaches a certain level (e.g., $\mathcal{L}/\lambda = 4.0$), the secrecy rate tends to stabilize. When $\mathcal{L}/\lambda = 5.0$, the proposed scheme outperforms Fixed IRS by 0.24 dB, FPA by 0.21 dB, and ZF by 0.44 dB. This performance stabilization indicates that the antenna's influence on the secrecy rate has reached a saturation point: beyond this point, further increasing the antenna size will only result in diminishing performance gains.

Finally, the relationship between the number of channel paths (L) and the secrecy rate is shown in Fig. 9. As the number of channel paths increases, the proposed scheme can leverage more diverse channel state information, leading to a continuous improvement in the secrecy rate. It can be observed from the figure that the ZF algorithm exhibits poor security performance when the number of paths is low. The main reason for this is that the rank of the channel matrix is lower than the number of transmit/receive antennas, which results in the matrix being

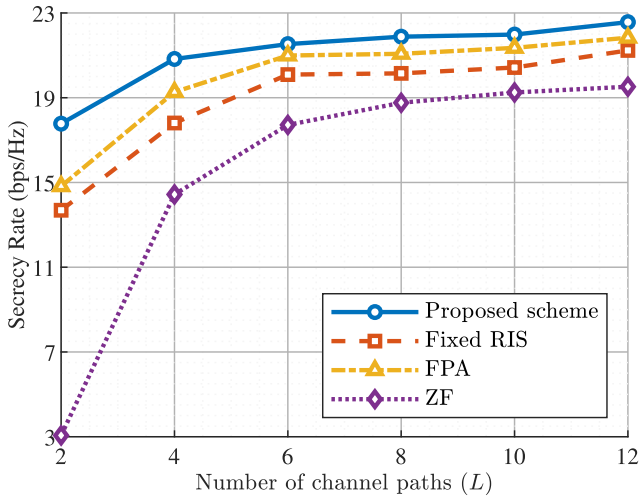

Fig. 9. Secure rate R_{sec} versus number of channel paths.

non-invertible or the pseudo-inverse calculation being inaccurate. A low-rank matrix cannot provide sufficient spatial degrees of freedom to separate signals. When the number of channel paths reaches L=8, the secrecy rate tends to stabilize. At this critical point, the proposed scheme outperforms the Fixed IRS by 0.36 dB, the FPA by 0.16 dB, and the ZF by 0.67 dB, as clearly indicated by the visual annotations in the figure. This stabilization suggests that the channel paths' contribution to the secrecy rate reaches a saturation point, where further increases in path numbers yield diminishing gains in performance.

V. Conclusion

This paper focused on an ISAC system for a single-target and single-user case, which was assisted by an intelligent reflecting surface and MA. The objective was to maximize the secure rate under the joint optimization of the communication beamformer at the transmitter, the sensing covariance matrix, the phase shifts of IRS, and the position of the MA. To solve this non-convex problem, a PSO-based alternating algorithm was adopted. Finally, the simulation results demonstrated that the proposed scheme can achieve good effectiveness compared with other benchmarking schemes.

References

[1] F. Liu et al., "Integrated sensing and communications: Toward dual-functional wireless networks for 6G and beyond," *IEEE J. Sel. Areas Commun.*, vol. 40, no. 6, pp. 1728–1767, Jun. 2022.
[2] X. Yang, Z. Wei, J. Xu, Y. Fang, H. Wu, and Z. Feng, "Coordinated transmit beamforming for networked ISAC with imperfect CSI and time synchronization," *IEEE Trans. Wireless Commun.*, vol. 23, no. 12, pp. 18019–18035, Dec. 2024.
[3] Q. Zhu, M. Li, R. Liu, and Q. Liu, "Cramér-Rao bound optimization for active IRS-empowered ISAC systems," *IEEE Trans. Wireless Commun.*, vol. 23, no. 9, pp. 11723–11736, Sep. 2024.
[4] D. Zhang et al., "Integrated Sensing and Communications Over the Years: An Evolution Perspective," 2025, *arXiv:2504.06830*.
[5] Y. Cui, X. Cao, G. Zhu, J. Nie, and J. Xu, "Edge perception: Intelligent wireless sensing at network edge," *IEEE Commun. Mag.*, vol. 63, no. 3, pp. 166–173, Mar. 2025.
[6] D. Wen et al., "Task-oriented sensing, computation, and communication integration for multi-device edge AI," *IEEE Trans. Wireless Commun.*, vol. 23, no. 3, pp. 2486–2502, Mar. 2024.
[7] X. Cao, Z. Lyu, G. Zhu, J. Xu, L. Xu, and S. Cui, "An overview on over-the-air federated edge learning," *IEEE Wireless Commun.*, vol. 31, no. 3, pp. 202–210, Jun. 2024.
[8] Z. Liu et al., "Integrated sensing and edge AI: Realizing intelligent perception in 6 G," *IEEE Commun. Surveys Tut.*, early access, 2025.
[9] Z. Wang, K. Huang, and Y. C. Eldar, "Spectrum breathing: Protecting over-the-air federated learning against interference," *IEEE Trans. Wireless Commun.*, vol. 23, no. 8, pp. 10058–10071, Aug. 2024.
[10] Z. Wang, Q. Zeng, H. Zheng, and K. Huang, "Revisiting outage for edge inference systems," 2025, *arXiv:2504.03686*.
[11] B. K. Chalise, M. G. Amin, and B. Himed, "Performance tradeoff in a unified passive radar and communications system," *IEEE Signal Process. Lett.*, vol. 24, no. 9, pp. 1275–1279, Sep. 2017.
[12] F. Liu, Y.-F. Liu, A. Li, C. Masouros, and Y. C. Eldar, "Cramér–Rao bound optimization for joint radar-communication beamforming," *IEEE Trans. Signal Process.*, vol. 70, pp. 240–253, 2022.
[13] Y. Liu, H.-H. Chen, and L. Wang, "Physical layer security for next generation wireless networks: Theories, technologies, and challenges," *IEEE Commun. Surveys Tuts.*, vol. 19, no. 1, pp. 347–376, Firstquarter 2017.
[14] Y. Zou, J. Zhu, X. Wang, and L. Hanzo, "A survey on wireless security: Technical challenges, recent advances, and future trends," *Proc. IEEE*, vol. 104, no. 9, pp. 1727–1765, Sep. 2016.
[15] J. Zou, C. Masouros, F. Liu, and S. Sun, "Securing the sensing functionality in ISAC networks: An artificial noise design," *IEEE Trans. Veh. Technol.*, vol. 73, no. 11, pp. 17800–17805, Nov. 2024.
[16] K. Ren, H. Su, and Q. Wang, "Secret key generation exploiting channel characteristics in wireless communications," *IEEE Wireless Commun.*, vol. 18, no. 4, pp. 6–12, Aug. 2011.
[17] K. Cao, et al., "Improving physical layer security of uplink NOMA via energy harvesting jammers," *IEEE Trans. Inf. Forensics Secur.*, vol. 16, pp. 786–799, 2021.
[18] B. He, F. Wang, and J. Cheng, "Joint secure transceiver design for integrated sensing and communication," *IEEE Trans. Wireless Commun.*, vol. 23, no. 10, pp. 13377–13393, Oct. 2024.
[19] L. Zhu, W. Ma, and R. Zhang, "Modeling and performance analysis for movable antenna enabled wireless communications," *IEEE Trans. Wireless Commun.*, vol. 23, no. 6, pp. 6234–6250, Jun. 2024.
[20] G. Hu et al., "Movable antennas-assisted secure transmission without eavesdroppers' instantaneous CSI," *IEEE Trans. Mobile Comput.*, vol. 23, no. 12, pp. 14263–14279, Dec. 2024.
[21] L. Zhu, W. Ma, B. Ning, and R. Zhang, "Movable-antenna enhanced multiuser communication via antenna position optimization," *IEEE Trans. Wireless Commun.*, vol. 23, no. 7, pp. 7214–7229, Jul. 2024.
[22] J. Chen, K. Wu, J. Niu, Y. Li, P. Xu, and J. A. Zhang, "Spectral and energy efficient waveform design for RIS-assisted ISAC," *IEEE Trans. Commun.*, vol. 73, no.1, pp. 158–172, Jan. 2025.
[23] H. Zhou, Y.-C. Liang, R. Long, L. Zhao, and Y. Pei, "Reconfigurable intelligent surface for FDD systems: Design and optimization," *IEEE Internet Things J.*, vol. 10, no. 11, pp. 9607–9621, Jun. 2023.
[24] S. Kim, J. Wu, and B. Shim, "Efficient channel probing and phase shift control for mmWave reconfigurable intelligent surface-aided communications," *IEEE Trans. Wireless Commun.*, vol. 23, no. 1, pp. 231–246, Jan. 2024.
[25] T. Wang, F. Fang, and Z. Ding, "An SCA and relaxation based energy efficiency optimization for multi-user IRS-assisted NOMA networks," *IEEE Trans. Veh. Technol.*, vol. 71, no. 6, pp. 6843–6847, Jun. 2022.
[26] W. Zhang, K. Xiong, R. Zhang, P. Fan, and K. B. Letaief, "SEE maximization in RIS-aided network with RSMA: A PPO-SCF method," *IEEE Wireless Commun. Lett.*, vol. 13, no. 12, pp. 3315–3319, Dec. 2024.
[27] Y. Guo, et al., "Secrecy energy efficiency maximization in IRS-assisted VLC MISO networks with RSMA: A DS-PPO approach," *IEEE Trans. Wireless Commun.*, vol. 24, no. 8, pp. 6475–6489, Aug. 2025.
[28] C. Zhong, J. Yao, and J. Xu, "Secure UAV communication with cooperative jamming and trajectory control," *IEEE Commun. Lett.*, vol. 23, no. 2, pp. 286–289, Feb. 2019.
[29] J. Yao and J. Xu, "Joint 3D maneuver and power adaptation for secure UAV communication with CoMP reception," *IEEE Trans. Wireless Commun.*, vol. 19, no. 10, pp. 6992–7006, Oct. 2020.
[30] W. Lu et al., "Secure transmission for multi-UAV-assisted mobile edge domputing based on reinforcement learning," *IEEE Trans. Netw. Sci. Eng.*, vol. 10, no. 3, pp. 1270–1282, May/Jun. 2023.

[31] L. Guo, J. Jia, J. Chen, S. Yang, Y. Xue, and X. Wang, "RIS-aided secure A2G communications with coordinated multi-UAVs: A hybrid DRL approach," *IEEE Trans. Netw. Sci. Eng.*, vol. 11, no. 5, pp. 4536–4550, Sep./Oct. 2024.
[32] B. Ji, Y. Wang, L. Xing, C. Li, Y. Wang, and H. Wen, "IRS-driven cybersecurity of healthcare cyber physical systems," *IEEE Trans. Netw. Sci. Eng.*, vol. 10, no. 5, pp. 2564–2573, Sep./Oct. 2023.
[33] Y. Zhang et al., "Robust secure UAV communications with the aid of jamming beamforming," *IEEE Trans. Commun.*, vol. 73, no. 11, pp. 12205–12220, Nov. 2025.
[34] D. Zhou, L. Li, S. Gong, B. Gu, G. Chen, and D. Niyato, "Learning adaptive jamming and beamforming for hybrid IRS-assisted secure NOMA transmissions," *IEEE Trans. Commun.*, vol. 73, no. 11, pp. 12235–12247, Nov. 2025.
[35] J. Xu et al., "IRS-UAV assisted secure integrated sensing and communication," *IEEE Wireless Commun.*, vol. 31, no. 5, pp. 61–67, Oct. 2024.
[36] C. Jiang, C. Zhang, C. Huang, J. Ge, D. Niyato, and C. Yuen, "RIS-assisted ISAC systems for robust secure transmission with imperfect sense estimation," *IEEE Trans. Wireless Commun.*, vol. 24, no. 5, pp. 3979–3992, May 2025.
[37] P. Liu, Z. Fei, X. Wang, B. Li, Y. Huang, and Z. Zhang, "Outage constrained robust secure beamforming in integrated sensing and communication systems," *IEEE Wireless Commun. Lett.*, vol. 11, no. 11, pp. 2260–2264, Nov. 2022.
[38] J. Chu, R. Liu, M. Li, Y. Liu, and Q. Liu, "Joint secure transmit beamforming designs for integrated sensing and communication systems," *IEEE Trans. Veh. Technol.*, vol. 72, no. 4, pp. 4778–4791, Apr. 2023.
[39] D. Xu, X. Yu, D. W. K. Ng, A. Schmeink, and R. Schober, "Robust and secure resource allocation for ISAC systems: A novel optimization framework for variable-length snapshots," *IEEE Trans. Commun.*, vol. 70, no. 12, pp. 8196–8214, Dec. 2022.
[40] W. Wei, et al., "Cramér-Rao bound and secure transmission trade-off design for semi-IRS-enabled ISAC," *IEEE Trans. Wireless Commun.*, vol. 23, no. 11, pp. 15753–15767, Nov. 2024.
[41] J. Zhang, J. Xu, W. Lu, N. Zhao, X. Wang, and D. Niyato, "Secure transmission for IRS-aided UAV-ISAC networks," *IEEE Trans. Wireless Commun.*, vol. 23, no. 9, pp. 12256–12269, Sep. 2024.
[42] X. Yu, J. Xu, N. Zhao, X. Wang, and D. Niyato, "Security enhancement of ISAC via IRS-UAV," *IEEE Trans. Wireless Commun.*, vol. 23, no. 10, pp. 15601–15612, Oct. 2024.
[43] D. Li, Z. Yang, N. Zhao, Z. Wu, and T. Q. S. Quek, "NOMA aided secure transmission for IRS-ISAC," *IEEE Trans. Wireless Commun.*, vol. 23, no. 9, pp. 10911–10925, Sep. 2024.
[44] M. Hua, Q. Wu, W. Chen, O. A. Dobre, and A. L. Swindlehurst, "Secure intelligent reflecting surface-aided integrated sensing and communication," *IEEE Trans. Wireless Commun.*, vol. 23, no. 1, pp. 575–591, Jan. 2024.
[45] X. Yu, J. Xu, X. Qin, J. Tang, N. Zhao, and D. Niyato, "Multistatic cooperative sensing assisted secure transmission via IRS," *IEEE Trans. Wireless Commun.*, vol. 24, no. 7, pp. 5752–5764, Jul. 2025.
[46] W. Wei, X. Pang, C. Xing, N. Zhao, and D. Niyato, "STAR-IRS aided secure NOMA integrated sensing and communication," *IEEE Trans. Wireless Commun.*, vol. 23, no. 9, pp. 10712–10725, Sep. 2024
[47] T. Zhou et al., "Robust and secure beamforming design for STAR-RIS-enabled IoE ISAC systems," *IEEE Internet Things J.*, vol. 12, no. 7, pp. 8742–8758, Apr. 2025.
[48] Z. Yang, S. Zhang, G. Chen, Z. Dong, Y. Wu, and D. B. D. Costa, "Secure integrated sensing and communication systems assisted by active RIS," *IEEE Trans. Veh. Technol.*, vol. 73, no. 12, pp. 19791–19796, Dec. 2024.
[49] Y. Zhang, et al., "Secure wireless communication in active RIS-assisted DFRC systems," *IEEE Trans. Veh. Technol.*, vol. 74, no. 1, pp. 626–640, Jan. 2025.
[50] Q. Liu, Y. Zhu, M. Li, R. Liu, Y. Liu, and Z. Lu, "DRL-based secrecy rate optimization for IRS-assisted secure ISAC systems," *IEEE Trans. Veh. Technol.*, vol. 72, no. 12, pp. 16871–16875, Dec. 2023.
[51] L. Zhu, W. Ma, and R. Zhang, "Movable-antenna array enhanced beamforming: Achieving full array gain with null steering," *IEEE Commun. Lett.*, vol. 27, no. 12, pp. 3340–3344, Dec. 2023.
[52] W. Xiong, K. Zhong, Z. Xiao, J. Lin, and Q. Li, "Secure analog beamforming design for wireless communication systems with movable antennas," in *Proc. 2025 IEEE Int. Conf. Acoust., Speech, Signal Process.*, Hyderabad, India, 2025, pp. 1–5.
[53] N. Li, P. Wu, B. Ning, and L. Zhu, "Sum rate maximization for movable antenna enabled uplink NOMA," *IEEE Wireless Commun. Lett.*, vol. 13, no. 8, pp. 2140–2144, Aug. 2024.
[54] Y. Wu, D. Xu, D. W. K. Ng, W. Gerstacker, and R. Schober, "Movable antenna-enhanced multiuser communication: Jointly optimal discrete antenna positioning and beamforming," in *Proc. GLOBECOM 2023-2023 IEEE Glob. Commun. Conf.*, Kuala Lumpur, Malaysia, 2023, pp. 7508–7513.
[55] G. Hu et al., "Intelligent reflecting surface-aided wireless communication with movable elements," *IEEE Wireless Commun. Lett.*, vol. 13, no. 4, pp. 1173–1177, Apr. 2024.
[56] J. Xiao, Y. Liu, Y. Chen, X. Wu, and F. Hou, "Throughput maximization for movable antenna and IRS enhanced wireless powered IoT networks," in *Proc. 2024 IEEE Wireless Commun. Netw. Conf.*, Dubai, UAE, 2024, pp. 1–6.
[57] H. Wu, H. Ren, C. Pan, and Y. Zhang, "Movable antenna-enabled RIS-aided integrated sensing and communication," *IEEE Trans. Cogn. Commun. Netw.*, vol. 11, no. 5, pp. 2879–2892, Oct. 2025,
[58] H. Qin, W. Chen, Q. Wu, Z. Zhang, Z. Li, and N. Cheng, "Cramér-Rao bound minimization for movable antenna-assisted multiuser integrated sensing and communications," *IEEE Wireless Commun. Lett.*, vol. 13, no. 12, pp. 3404–3408, Dec. 2024.
[59] C. Jiang, C. Zhang, C. Huang, J. Ge, D. Niyato, and C. Yuen, "Movable antenna-assisted integrated sensing and communication systems," *IEEE Trans. Wireless Commun.*, vol. 24, no. 8, pp. 6397–6412, Aug. 2025.
[60] H. Wu, H. Ren, C. Pan, and Y. Zhang, "Movable antenna-enabled RIS-aided integrated sensing and communication," *IEEE Trans. Cogn. Commun. Netw.*, vol. 11, no. 5, pp. 2879–2892, Oct. 2025.
[61] W. Xiang, Y. Chen, X. Zhang, Z. Lu, and X. Wen, "Joint antenna position and transmit signal optimization for ISAC system with movable antenna array," in *Proc. IEEE 35th Int. Symp. Pers., Indoor Mobile Radio Commun.*, Valencia, Spain, 2024, pp. 1–6.
[62] W. Lyu, S. Yang, Y. Xiu, Z. Zhang, C. Assi, and C. Yuen, "Flexible beamforming for movable antenna-enabled integrated sensing and communication," in *Proc. IEEE 24th Int. Conf. Commun. Technol.*, Chengdu, China, 2024, pp. 1315–1320.
[63] W. Lyu, S. Yang, Y. Xiu, Z. Zhang, C. Assi, and C. Yuen, "Movable antenna enabled integrated sensing and communication," *IEEE Trans. Wireless Commun.*, vol. 24, no. 4, pp. 2862–2875, Apr. 2025.
[64] S. Zhang and R. Zhang, "Capacity characterization for intelligent reflecting surface aided MIMO communication," *IEEE J. Sel. Areas Commun.*, vol. 38, no. 8, pp. 1823–1838, Aug. 2020.
[65] Q. Wu and R. Zhang, "Beamforming optimization for wireless network aided by intelligent reflecting surface with discrete phase shifts," *IEEE Trans. Commun.*, vol. 68, no. 3, pp. 1838–1851, Mar. 2020.
[66] Y. Fang, S. Zhang, X. Li, X. Yu, J. Xu, and S. Cui, "Multi-IRS-enabled integrated sensing and communications," *IEEE Trans. Wireless Commun.*, vol. 72, no. 9, pp. 5853–5867, Sep. 2024.
[67] J. Zuo, Y. Liu, C. Zhu, Y. Zou, D. Zhang, and N. Al-Dhahir, "Exploiting NOMA and IRS in integrated sensing and communication," *IEEE Trans. Veh. Technol.*, vol. 72, no. 10, pp. 12941–12955, Oct. 2023.
[68] Z. Xiao, X. Pi, L. Zhu, X.-G. Xia, and R. Zhang, "Multiuser communications with movable-antenna base station: Joint antenna positioning, receive combining, and power control," *IEEE Trans. Wireless Commun.*, vol. 23, no. 12, pp. 19744–19759, Dec. 2024.

Xiaowen Cao (Member, IEEE) received the B.Eng. and Ph.D. degrees from the Guangdong University of Technology, Guangzhou, China, in 2017 and 2022, respectively. She is currently an Assistant Professor with the College of Electronics and Information Engineering, Shenzhen University, Shenzhen, China, and a Visiting Scholar with the Guangdong Provincial Key Laboratory of Future Networks of Intelligence, Shenzhen. Her research interests include edge learning, over-the-air computation, integrated sensing, communication, and computation. She is a recipient of the World's Top 2% Scientists by Stanford University, the Best Paper Award of IEEE JC&S 2024, and the eExemplary Reviewer for IEEE WCL. She was a Co-Chair of IEEE VTC-fall 2023 workshop on ISCC, and a TPC Co-Chair of IEEE WCNC/PIMRC 2024 workshop.

Peng Jiang received the M.S. degree in electronic information from the College of Electronics and Information Engineering, Shenzhen University, Shenzhen, China. His research interests include wireless communications and intelligent reflecting surface.

Guangxu Zhu (Member, IEEE) received the Ph.D. degree in electrical and electronic engineering from The University of Hong Kong, Hong Kong, in 2019. He is currently a Senior Research Scientist and the Deputy Director of network system optimization center with the Shenzhen Research Institute of Big Data, and an Adjunct Associate Professor with the Chinese University of Hong Kong, Shenzhen, China. His research interests include edge intelligence, semantic communications, and integrated sensing and communication. He is a recipient of the 2023 IEEE ComSoc Asia-Pacific Best Young Researcher Award and Outstanding Paper Award, the World's Top 2% Scientists by Stanford University, the "AI 2000 Most Influential Scholar Award Honorable Mention", the Young Scientist Award from UCOM 2023, the Best Paper Award from WCSP 2013, and IEEE JS&C 2024. He is an Associate Editor for top-tier journals in IEEE, including IEEE TRANSACTIONS ON MOBILE COMPUTING, IEEE TRANSACTIONS ON WIRELESS COMMUNICATIONS, and IEEE WIRELESS COMMUNICATIONS LETTERS. He is the Vice Co-Chair of the IEEE ComSoc Asia-Pacific Board Young Professionals Committee.

Yejun He (Senior Member, IEEE) received the Ph.D. degree in information and communication engineering from the Huazhong University of Science and Technology, Wuhan, China, in 2005. From 2005 to 2006, he was a Research Associate with the Department of Electronic and Information Engineering, The Hong Kong Polytechnic University, Hong Kong. From 2006 to 2007, he was a Research Associate with the Department of Electronic Engineering, Faculty of Engineering, The Chinese University of Hong Kong, Hong Kong. In 2012, he joined the Department of Electrical and Computer Engineering, University of Waterloo, Waterloo, ON, Canada, as a Visiting Professor. From 2013 to 2015, he was an Advanced Visiting Scholar (Visiting Professor) with the School of Electrical and Computer Engineering, Georgia Institute of Technology, Atlanta, GA, USA. From 2023 to 2024, he was an Advanced Research Scholar (Visiting Professor) with the Department of Electrical and Computer Engineering, National University of Singapore, Singapore.

Since 2006, Dr. He has been a faculty of Shenzhen University, where he is currently a Full Professor with the College of Electronics and Information Engineering, Shenzhen University, Shenzhen, China, the Director of Sino-British Antennas and Propagation Joint Laboratory of Ministry of Science and Technology, China, the Director of the Guangdong Engineering Research Center of Base Station Antennas and Propagation, and the Director of the Shenzhen Key Laboratory of Antennas and Propagation. He was selected as an Expert with Special Government Allowance from the State Council in China, and a Leading Talent in the "Guangdong Special Support Program" in 2024. He was promoted to the Shenzhen "Pengcheng Scholar" Distinguished Professor in 2020. He has authored or coauthored more than 350 refereed journal and conference papers and seven books. He holds more than 30 patents. His research interests include wireless communications, antennas, and radio frequency. Dr. He was a recipient of the Shenzhen Overseas High-Caliber Personnel Level B (Peacock Plan Award B), Shenzhen High-Level Professional Talent (Local Leading Talent), Second Prize of Shenzhen Science and Technology Progress Award in 2017, Three Prize of Guangdong Provincial Science and Technology Progress Award in 2018, Second Prize of Guangdong Provincial Science and Technology Progress Award in 2023, and the 10th Guangdong Provincial Patent Excellence Award in 2023. He is the Chair of IEEE Antennas and Propagation Society-Shenzhen Chapter and obtained the 2022 IEEE APS Outstanding Chapter Award. He was a Technical Program Committee Member or a Session Chair for various conferences, including the IEEE Global Telecommunications Conference, the IEEE International Conference on Communications, the IEEE Wireless Communication Networking Conference, and the IEEE Vehicular Technology Conference. He was the TPC Chair for IEEE ComComAp 2021 and the General Chair for IEEE ComComAp 2019. He was selected as a Board Member of the IEEE Wireless and Optical Communications Conference. He was the TPC Co-Chair for WOCC 2023/2022/2019/2015, APCAP 2023, UCMMT 2023, ACES-China2023, and NEMO 2020. He was the Publicity Chair of several international conferences such as the IEEE PIMRC 2012. He was an Executive Chair of 2024/2025 IEEE International Workshop of Radio Frequency and Antenna Technologies and is acting as an Executive Chair of 2026 IEEE International Conference of Radio Frequency and Antenna Technologies. He is the Principal Investigator for more than 40 current or finished research projects, including the National Natural Science Foundation of China, the Science and Technology Program of Guangdong Province, and the Science and Technology Program of Shenzhen City. He was a Reviewer for various journals, such as IEEE TRANSACTIONS ON VEHICULAR TECHNOLOGY, IEEE TRANSACTIONS ON COMMUNICATIONS, the IEEE TRANSACTIONS ON INDUSTRIAL ELECTRONICS, IEEE TRANSACTIONS ON ANTENNAS AND PROPAGATION, IEEE WIRELESS COMMUNICATIONS, the IEEE COMMUNICATIONS LETTERS, the *International Journal of Communication Systems*, and *Wireless Personal Communications*.

Dr. He is a Fellow of IET, and a Fellow of China Institute of Communications. He is an Associate Editor for IEEE TRANSACTIONS ON VEHICULAR TECHNOLOGY, IEEE TRANSACTIONS ON ANTENNAS AND PROPAGATION, IEEE TRANSACTIONS ON MOBILE COMPUTING, IEEE ANTENNAS AND WIRELESS PROPAGATION LETTERS, IEEE ANTENNAS AND PROPAGATION MAGAZINE, *International Journal of Communication Systems*, *China Communications*, and *ZTE Communications*.

Mohsen Guizani (Fellow, IEEE) received the B.S. (with distinction), M.S., and Ph.D. degrees in electrical and computer engineering from Syracuse University, Syracuse, NY, USA.

He was with different institutions in the USA. He is currently a Professor of machine learning with the Mohamed Bin Zayed University of Artificial Intelligence (MBZUAI), Abu Dhabi, UAE. He is the author of 11 books, more than 1000 publications and several US patents. His research interests include applied machine learning and artificial intelligence, smart city, Internet of Things, intelligent autonomous systems, and cybersecurity. He was listed as a Clarivate Analytics Highly Cited Researcher in computer science from 2019 to 2022.

Dr. Guizani has won several research awards including the "2015 IEEE Communications Society Best Survey Paper Award", Best ComSoc Journal Paper Award in 2021, and 5 Best Paper Awards from ICC and Globecom Conferences. He was the recipient of the 2017 IEEE Communications Society Wireless Technical Committee Recognition Award, 2018 AdHoc Technical Committee Recognition Award, and the 2019 IEEE Communications and Information Security Technical Recognition Award. He was the Editor-in-Chief of IEEE NETWORK and is serving on the Editorial Boards of many IEEE Transactions and Magazines. He was the Chair of the IEEE Communications Society Wireless Technical Committee and the Chair of the TAOS Technical Committee. He was the IEEE Computer Society Distinguished Speaker and is the IEEE ComSoc.